THE UNIVERSITY OF MICHIGAN

INDUSTRY PROGRAM OF THE COLLEGE OF ENGINEERING

THE SIMULATION OF A GUST IN A WIND TUNNEL BY MEANS OF A MOVING BUMP

Louis C. Garby

A dissertation submitted in partial fulfullment
of the requirements for the degree of
Doctor of Philosophy in the
University of Michigan
1957

December, 1957

IP-260

PREFACE

The author wishes to acknowledge the help given by the doctoral committee composed of Professors A. M. Kuethe, Co-chairman, J. D. Schetzer, Co-chairman, W. C. Nelson, E. J. Lesher, and R. C. Bartels, and particularly the help of Professors A. M. Kuethe and J. D. Schetzer. Dr. R. Mills and Mr. E. Johnson of the Aeronautical Research Laboratory of the U.S.A.F. also gave valuable assistance through their suggestions and sympathetic understanding of the work involved.

The sponsorship of the United States Air Force for the work reported herein is also acknowledged. The Engineering Research Institute of the University of Michigan held this contract, AF 33 (616)316, and Professor A. M. Kuethe was the project supervisor.

TABLE OF CONTENTS

LIST OF FIGURES

LIST OF FIGURES CONT'D

LIST OF FIGURES CONT'D

INTRODUCTION

With increasing size, range, and complexity of aircraft, it is becoming important to determine more closely the effects of atmospheric gusts upon aircraft. Experimental information has been obtained largely in two ways: by full-scale flight tests through turbulent air, and from experimental model techniques in which the gust is simulated. Atmospheric turbulence is made up of a large number of gusts statistically distributed in intensity and scale. A particular cross section of the atmosphere through which an aircraft flies is repeatable, therefore, only in its statistical aspects. Flight-test work can only, in general, give a gross response and will not easily yield details as to the exact manner in which the gust acts upon the aircraft.

The experimental approach has been pursued largely by three methods: the use of a whirling arm, flying a free flight model through a vertical gust, and wind tunnel tests on an oscillating wing.

To provide the designer with more information, and to point the way for theoretical work, another experimental approach which simulated the passage of a wing through a gust was devised. This work is reported herein.

UNSTEADY AERODYNAMIC EFFECTS

If the flow field about an aircraft is changing rapidly, certain nonstationary effects come into play that cause the lift and moment on the aircraft to depart from their "quasi-steady" values. The term "quasi-steady lift" is used to denote that portion of the unsteady lift which is equal to the steady-state value corresponding to the flow configuration at that instant. The difference between the true dynamic lift and the quasi-steady value is called the lift lag.

The details of the various contributions to the lift lag are not understood for wing-body-tail combinations in which interference effects play a prominent role. For a wing at subsonic speed, the lift lag is produced by the wake that accompanies the time-varying circulation and by the inertial reaction of the air. For simple plan forms, the so-called "wake lift" and "apparent-mass" lift can be predicted from the theory of thin airfoils. For a wing moving through a severe gust, the lift lag is known to be important. For a complete airplane with all interference effects considered, it is expected that the lift lag will also be an important factor. The lift lag is an essential feature of the gust problem; therefore, gust-simulation equipment must include instrumentation which is adequate for accurate measurement of the lift lag.

Tests of gust-simulation equipment and its use in determining the unsteady lift on a constrained two-dimensional wing are described in the following sections. The theory for this case is well understood and has served as a guide for developing the instrumentation necessary to measure the lift.

PREVIOUS WORK ON GUST SIMULATION AND RELATED PROBLEMS

Among the earlier experiments on unsteady flow are those described in Reference 17. An airfoil was set in motion in a water tank and the flow pattern was made visible by shining a light on suspended oil globules. The circulation build-up during the first few chords of airvoil travel was calculated from the motion of the globules. Direct force measurements were obtained on a wing near the stalling angle and during rotation at a rate of one degree in 2.5 chords of wing travel (Reference 7). The circulation build-up on a wing was determined by taking hot-wire measurements of the flow pattern around the tip-trailing vortices as the wing passed through an updraft of known profile (Reference 12).

Experiments in unsteady aerodynamics have been confined mostly to the measurement of forces and moments on models which are oscillated in a wind tunnel. The frequency information thus obtained is used to calculate arbitrary periodic motions by applying the superposition principle. Experiments of this type have been reported in the literature as early as twenty years ago, and they are currently being performed in ever-increasing numbers. Representative experiments on wings, bodies, and wing-body combinations are described in References 1, 2, 3, 8, and 9.

It is believed that the only facilities presently in use for simulating the effect of atmospheric gusts are of the NACA Langley Field type, in which a model is projected through an updraft of controlled velocity distribution. The resulting motion is observed photographically (References 5 and 6).

EXPERIMENTAL TECHNIQUES

The following qualifications or criteria were established to devise an experimental technique to check theoretical predictions and to provide design data.

Repeatability

The gust pattern and response must be repeatable and these conditions must be capable of controlled variation.

Test Configuration

The mechanism of the gust should be such that the model is either entering or emerging from the gust. It is in this transitional period that the lift lag occurs.

Gust Structure

The gust structure preferably should be a monotonic and rapid change in angle of attack. A monotonic variation will in general be more reproducible, and the calculations necessary for a comparison with theory will be less involved than for more complicated gust structures. The more rapid the variation of angle of attack, the greater will be the lift lag, and hence greater accuracy will be obtainable in its measurement.

Test Velocity

For accurate comparison with theory the mean velocity in the windstream direction should remain as constant as possible, so that the gust will cause an angle-of-attack change which can be reproduced in a quasi-steady manner.

Quasi-Steady Effect

The mechanism producing the gust should be such that the gust pattern can be frozen at various degrees of penetration of the model. Quasi-steady measurements can then be made and the lift lag determined experimentally.

It was felt that along with the above conditions the model should be fixed in the tunnel while the gust passes over it, rather than the reverse. The instrumentation for the measurement of forces and for control of angle of attack is much simpler for a fixed than for a moving model.

To carry out this program, two wind tunnels were used. Initial development of the Vortex and Moving Bump Gust Generator models was carried out in a small open-return tunnel having a nominal test-section dimension of 21 x 29 inches. A sketch of the tunnel with pertinent dimensions is given in Figure 1. Details of the configuration are given in Appendix I. A second tunnel was used to extend the results of the Moving Bump Gust Generator model by increasing the Reynolds number. A sketch of this tunnel is shown in Figures 2a and 2b, and details of its configuration are given in Appendix I.

The passage of a gust across a fixed model may be achieved in two ways: (1) a continuous variation of the boundary conditions at the tunnel wall will cause an angle-of-attack change to sweep past the model; (2) a disturbance placed in the flow upstream of the model will be carried past the model by the tunnel flow.

The technique reported here is the first of the above; the second technique is reported in References 13 and 14. The test configurations and testing techniques are the same for both tunnels. The gust was generated by moving a two-dimensional bump along the floor of the tunnel. The flow field which passed over the model, shown schematically in Figure 3, simulated the emergence of the model from a gust, whose severity depended upon

the rate of movement of the bump and the air speed.

Sketches and photographs of the bump are shown in Figure 4. In order to reduce the inertia of the system, the bump was a light structure made of sheet aluminum. The bump rode upon rails, which were machined from iron and were bolted to the floor of the tunnel. Ball bearings served as the rollers and were used to restrain the bump in all directions except along the tunnel axis.

It was necessary to accelerate the bump to test speed in as short a distance as possible so that the gust profile would pass across the wing at a constant speed. It then traveled the remainder of the distance at constant speed. The energy required to accelerate the bump was obtained by locking it in a forward position and stretching 5/8-inch-diameter rubber shock chords attached to the aft frame. With release of the lock, the bump accelerated rapidly to test speed and then traveled along its path at nearly a constant speed. Control of the bump speed was obtained by the extension of the shock chords.

At the end of its path the bump struck a piston extending from an air cylinder. The energy of the moving bump was dissipated by throttling the compressed air in the cylinder through an orifice to the atmosphere. Figure 5 is a schematic diagram of the system.

The gust effect studied in this work was that of the normal force response to a known angle of attack change. To measure the gust effect, the following measurements were made: position of bump in test section, angle of flow, wind speed, and normal force on the wing model.

The position of the bump was measured by connecting the bump to a potentiometer. The bump position could be determined within an accuracy of ± 0.05 inch. Details of the system and circuit are given in Appendix II-A. Figure 6 shows bump histories for a series of tests. It may be

seen that the bump reached its speed within approximately 1/2 chord and that the speed remained constant thereafter.

The angle of flow was measured by means of a hot-wire anemometer with an "X probe." The probe position was reproducible to ± 0.1 degree. A sensitivity of 0.02 degree was obtained by the electrical equipment. Methods of mounting and the circuit diagrams are given in Appendix II-B. Typical angle-of-attack plots for the Moving Bump Gust Generator are given in Figure 7.

Dynamic data were initially recorded on a dual beam DuMont oscilloscope with a Polaroid-Land camera which photographed the face of the scope. In the later tests, particularly those in the 5- x 7-foot tunnel, a Consolidated recording oscillograph was used.

The normal forces were measured by a single-component balance. The balance converted the normal force into either a rotational or translational displacement which was amplified and measured by means of a Schaevitz Linear Variable Differential Transformer. Details of the balance are given in Appendix II-C.

Prior to and immediately following each series of dynamic runs, quasi-steady and calibration runs were made to help determine the cause of possible inconsistencies which sometimes occurred in the dynamic data.

LIFT LAG THEORY

A wind proceeding past an airfoil at a constant speed but undergoing an angle of attack change will cause a change in wing lift with time. With the change in lift there is a change in circulation about the wing. As in steady wing lift theory, the rearward stagnation point remains at the trailing edge (Kutta condition). In accordance with the Helmholtz theorem, vortices of equal strength but opposite to those created about the wing will be shed into the wake. The shed vortices make up a time dependent sheet in the wake and their flow field will induce a lift on the wing.

The dynamic lift is expressed by the equation (see Reference 11, p. 382, eq. 16a)

$$L' = \underbrace{-\rho \frac{\partial}{\partial t} \int_{-2b}^{2b} \gamma_Q \, x dx}_{L'_a} + \underbrace{\rho V_\infty \Gamma_Q}_{L'_Q} + \underbrace{\rho V_\infty \int_{2b}^{\infty} \frac{\gamma(\xi)}{\sqrt{(\xi/2b)^2 - 1}} d\xi}_{L'_w} \quad (1)$$

$$L' = L'_a + L'_Q + L'_w$$

L'_Q is the quasi-steady lift response obtained by fixing the gust pattern across the wing and neglecting the effect of the vorticity in the wake.

L'_a is the apparent mass lift.

L'_w is called the wake lift. It is the lift response from the presence of a wake vortex sheet.

The method for obtaining each of these components is outlined in the following paragraphs.

Quasi-Steady Lift

g(x) represents an arbitrary distribution of normal velocity over the airfoil as shown in Figure 8a. The quasi-steady circulation Γ_Q is given by (Reference 4, p. 41, eq. 8, 14)

$$\Gamma_Q = 2\pi b \sum_{n=1}^{n=\infty} \frac{n\, B_n}{b^{n+1}} \tag{2}$$

where:

$$\frac{n\, B_n}{b^{n+1}} = \frac{2}{\pi} \int_{-\pi}^{\pi} g(x) \sin n\theta \sin \theta d\theta \tag{3}$$

with:

$$x = 2b \cos \theta$$

Apparent Mass Lift

The term γ_Q is needed to evaluate the apparent mass lift integral, Reference 4, p. 41, eq. 8.15.

$$\gamma_Q = \sum_{n=1}^{n=\infty} \frac{n\, B_n}{b^{n+1}} \left(\frac{1 - \cos n\theta}{\sin \theta} \right) \tag{4}$$

Wake Lift

The wake vortex distribution is related to the quasi-steady circulation Γ_Q by means of the Helmholtz theorem (Figure 9). The vorticity distribution in the wake following a unit jump in Γ_Q was found by Wagner, Reference 16. Using this vorticity distribution $\gamma(\xi)$ in the last term of equation (1), Karman-Sears and others were able to express L'_W as follows, Reference 11.

$$L'_W(\sigma) = - \rho V_\infty \Gamma \phi(\sigma) \tag{5}$$

(σ) is the nondimensional time $V_\infty t/2b$ and represents the half chords of travel following a unit jump in Γ_Q.

Jones fitted the following formula to the numerical value of $\phi(\sigma)$, Reference 9

$$\phi(\sigma) = 0.165\, e^{-0.0455\sigma} + 0.335\, e^{-0.0300\sigma} \tag{6}$$

The lift for a continuously varying Γ_Q is then found by linear superposition (Duhamel integration). For a continuously varying Γ_Q, the wake lift L'_w may be written as:

$$L'_w(\sigma) = -\rho V_\infty \int_0^\sigma \dot{\Gamma}_Q(\nu)\, \phi(\sigma-\nu)\, d\nu = -\rho V_\infty \left\{\dot{\Gamma}_Q * \phi\right\} \tag{7}$$

where:

$$\dot{\Gamma}_Q = \frac{\partial \Gamma_Q}{\partial \sigma}$$

In order to make a comparison between the experimental results and theoretical work, a correction must be made to the theory for the effect of the top and bottom wind tunnel walls. A mathematical model which will produce the experimental condition of a wake and two walls requires an infinite set of image vortex sheets. This model is shown in a simplified manner in Figure 10. The walls reduce the influence of the wake upon the airfoil. As a wake vortex moves downstream, the image vortices will contribute a velocity component in the opposite direction to that of the wake vortex.

The ratio $\bar{v}$ for a vortex midway between two parallel walls to that for a vortex having boundaries at infinity $\bar{v}_o$ is given by (Reference 15, p. 76).

$$\frac{\bar{v}}{\bar{v}_o} = \frac{\pi x}{a} \times \frac{1}{\sinh \pi x/a} \tag{8}$$

See Figure 11 for a definition of x and a.

The effect of the tunnel walls upon the wake lift for a gust step

input of $\Gamma = 1$ was determined to a first approximation as follows. The normal velocity distribution across the wing caused by a vortex element in the wake was assumed to be constant, and equal to that at the mid-chord position.

The normal velocity $\bar{v}'_o$ at the mid-chord point of the wing was computed for a wake vortex sheet formed by a step gust input $\Gamma = 1$. Similarly, the normal velocity $\bar{v}'$ was determined for this same vortex sheet in the presence of a wall of infinite extent. The ratio $\frac{\bar{v}'}{\bar{v}'_o}(\sigma)$ applies strictly at the mid-chord of the wing, but it was assumed to hold across the chord. Thus it was assumed that the normal velocity distribution across the wing was reduced by a constant ratio or percentage for each value of wake distance σ. It follows that the circulation about the wing caused by the wake vortex was reduced by this same ratio in comparison with the circulation obtained for a wake vortex sheet with boundaries at infinity. The wake lift was therefore reduced by a factor $\bar{v}'/\bar{v}'_o$ (approximately) from that calculated by the Wagner function.

The above correction considers the change in normal velocity distribution across the wing caused by the attenuating effect of the tunnel walls. The influence of the tunnel walls on the wing's lift lag is considered negligible for the following reasons. The lift lag is obtained by subtracting the quasi-steady lift from the dynamic lift. Both of these terms are of the same order of magnitude. The lift lag is approximately ten percent of their value. Thus any effect of the tunnel walls will be largely canceled in the subtractive process. Furthermore, the chord length of the wing was twenty percent of the height of the tunnel. For a wing of this size, the tunnel wall effects are relatively small.

The indicial admittance of equation (5) was multiplied by $\frac{\bar{v}'}{\bar{v}'_o}(\sigma)$, to calculate the wake lift. The equation for the wind tunnel wake lift is:

$$L'_w = - \rho V_\infty \Gamma_Q \phi'(\sigma) \tag{9}$$

where:

$$\phi'(\sigma) = \phi(\sigma) \frac{\bar{v}'}{\bar{v}'_o} (\sigma)$$

The apparent mass lift is given by the term

$$- \rho \frac{\partial}{\partial t} \int_{-2b}^{2b} \gamma_Q \, x dx$$

of equation (1). Calculations from the experimental data were made by the following method. The change in angle of attack across the wing is nearly linear for any gust position on the wing. A linear variation of normal velocity chord position is assumed for the mathematical model of the gust input (Figure 8b). The equation for the gust input is:

$$g(x) = \frac{U}{8b} (V_B t - 2b - x) \tag{10}$$

where:

U = change in normal velocity occurring in two chord lengths

V_B = bump speed

$2b$ = one-half the airfoil chord

x = distance from the center of the airfoil chord

The apparent mass lift equation may be solved with equations (3), (4), and (10). The result is

$$L'_a = - \pi \rho \frac{b}{2} V_B U \tag{11}$$

Values V_B and U are determined from the experimental data at various time intervals and the apparent mass lift calculated therefrom.

The theoretical lift lag with and without the wall boundary correction is compared in Figure 12. Quasi-steady data from one of the runs were used to calculate the lift lag.

TEST RESULTS AND DISCUSSION

The theory outlined in the previous section predicts a lift lag given by:

$$L_L = L' - L'_Q = L'_a + L'_w$$

where:

L_L = lift lag

L' = dynamic lift = $L'_a + L'_Q + L'_w$

L'_Q = quasi-steady lift

The experimental lift lag was obtained by subtracting the quasi-steady lift force from the dynamic lift force at the same bump position. Theoretical lift lag used for comparison was obtained by computing the wake lift and the apparent mass lift from the quasi-steady experimental data.

The first of the moving bump tests was conducted in the small open-return tunnel described in Appendix I. The wing had a chord of 6 inches and a span of 12 inches; two-dimensional flow was maintained by use of end plates. The angle-of-attack distribution for the gust passing over the wing is shown in Figure 7. This distribution passed over the wing at the speed at which the bump moved. Figure 6 shows that the bump was rapidly accelerated to a constant speed.

Under dynamic conditions, the normal velocity distribution differs from the quasi-steady pattern because of the motion of the bump (see Figure 13). The dynamic streamlines were flatter; therefore the gust should be less intense than was indicated by quasi-steady tests. Figure 7 shows the effect of the bump upon angle-of-attack change in the stream. A change of 8 degrees occurred in 4 chord lengths for both tests.

Preliminary tests were made in the 21- x 29-inch tunnel. Test results are shown for tunnel speeds of 27.9 fps and 44.4 fps, with respective bump speeds of 9.6 fps and 10.1 fps. For these tests, the lift response of the quasi-steady and dynamic cases plotted as a function of time are shown in Figure 14. The curve for bump position shown on the same plot made it possible to transfer the data to distance coordinates. The experimental and theoretical lift lags are given in Figure 15. There is good agreement between the curves, but the experimental data indicate a higher peak than the theory. The above tests were conducted at a Reynolds number of 93,000 and 148,000.

To extend the Reynolds number, tests were continued in the 5- x 7-foot tunnel. Tests were made at tunnel speeds of 72.5, 60, 35, and 20 fps. At the lower two speeds, a superimposed oscillation was picked up by the wing. The oscillation was such that the data were invalid. Figure 16 shows the quasi-steady and dynamic normal force response and bump position as a function of time for a tunnel speed of 60 fps with a bump speed of 14.2 fps, and a tunnel speed of 72.5 fps with bump speeds of 12.3 and 14.3 fps.

The comparison between the experimental and theoretical lift lag results are shown in Figure 17. Results of tests made in the 21- x 29-inch tunnel (Figure 15) and the 5- x 7-foot tunnel (Figure 17) are compared. The general character of the theoretical lift lag response followed the experimental lift lag very well. In all cases the theoretical results indicate an earlier rise in lift lag than is shown by experiment. By assuming a constant bump speed throughout the motion, it was possible to get better agreement between the experimental and theoretical lift lag in the first part of the curve.

For the 21- x 29-inch tunnel, the maximum value of experimental lift lag is larger than the theoretical by about 12%. For the 5- x 7-foot tun-

nel at 72.5 fps, the maximum values of theoretical and experimental lift lag were nearly the same. At 60 fps this effect was reversed, and the maximum value of the theoretical lift lag was larger than the experimental value. Other data taken at this tunnel speed indicated that there was a slight rubbing action occurring in the balance. This rubbing could occur if the Schaevitz transformer core was not centered properly in the transformer. The rubbing would tend to reduce the experimental lift lag and shift the experimental curve to the right. The relatively larger maximum experimental lift lag noted in the 21- x 29-inch tunnel tests might possibly be associated with the manner of mounting the wing. The wing was mounted at one end and acted as a cantilever beam (see Appendix II). With one end free, the inertia of the wing in bending might possibly add to the lift response for the dynamic case. In the 5- x 7-foot tunnel tests, this wing tip was restrained.

The effect of the tunnel walls on the theoretical lift lag is shown in Figure 12. The quasi-steady conditions for the theoretical lift lag was obtained from the 5- x 7-foot tunnel tests at V = 72.5 fps and a bump speed of 14.2 fps. The difference between the two curves is not too large during the initial rise of the lift lag response. However, by the time the maximum value of the lift lag has been reached and for a considerable time thereafter the correction from the wind tunnel walls is an important term.

The vortex system that leaves the endplates is shaped like a horseshoe, with its ends attached to the trailing edge of the endplates. For ease in calculating the theoretical lift the wake system was assumed two dimensional. Because of the geometry of the endplates, the error induced by this assumption is of the order of 5% at the point of maximum lift lag. This is within the error of the experiment. The agreement between theoretical and experimental lift lags was good.

CONCLUSIONS

The theoretical and experimental results agreed within the experimental errors throughout the range of tests. These tests were conducted in two different wind tunnels and over a Reynolds number range from 93,000 to 465,000. Over this range the experimental tests compared uniformly with the theory. No indication of trouble was observed which might limit the tests to a low Reynolds number.

The correction of the theory for the tunnel wall effect was an important factor. Without this correction, there was considerable deviation between experiment and theory in the trend of the lift lag force with time, particularly after the time at which the peak force was reached.

APPENDIX I

DESCRIPTION OF TEST TUNNELS

A. 21- x 29-Inch Tunnel

Initial test work for both the Vortex and Moving Bump Gust Generators was done in a small open-return tunnel. A sketch of the tunnel is shown in Figure 1. Data pertinent to this tunnel are listed below:

speed range: 0 - 65 feet per second
turbulence level: 0.03% at V = 50 fps
contraction ratio: 16
nominal test section size: 21 inches high
29 inches wide
100 inches long

The tunnel was constructed so that test sections were interchangeable. One test section contained the Vortex Gust Generator, and another contained a Moving Bump Gust Generator.

Tunnel speed was controlled by changing the revolutions per minute of a fixed pitch fan. A Reeves Vari-speed drive was the mechanism of speed change.

B. 5- x 7-Foot Tunnel

Work was continued with the Moving Bump Gust Generator on a larger scale. For this, a tunnel was constructed as a joint effort by the Air Force and the University. Previous experience had indicated the importance of keeping the turbulence level as low as possible. Figure 2 shows the plan view and dimensions at critical stations.

Data pertinent to this tunnel are:

speed range: 0 - 250 feet per second
turbulence level: 0.02% at V = 100 fps
0.035% at V = 200 fps

contraction ratio: 15
test section size: 5 feet high
7 feet wide
25 feet long
power plant: Ward-Leonard drive, 1250 horsepower available, 300 horsepower required at maximum condition
fan: fixed pitch, 10 blades of laminated wood
maximum diffuser angle: 5.5 degrees except in rapid expansion section
settling chamber: 5 screens, 30-mesh wire of 0.075-inch diameter spaced 30 inches apart. After the last screen there is a distance of 10 feet before the nozzle starts.

An artist's sketch of the tunnel is shown in Figure 2a. Rails on which the moving bump traveled were covered by the bottom corner fillets when gust tests were not being made.

APPENDIX II

INSTRUMENTATION DETAILS

A. Bump-Position Indicator

To indicate the position of the bump in the test section for both dynamic and quasi-steady tests, a system as shown in Figure 18 was used. A cable attached to the nose of the bump was wrapped around the drum of a 10-turn potentiometer. The motion of the bump rotated the potentiometer.

To position the bump for quasi-steady measurements, holes were drilled through the floor of the test section at given distances downstream. A tight pin inserted through the hole would allow the bump to rest at a known position. These holes were located with an accuracy of $\pm$ 0.05 inch.

B. Angle-of-Attack Measurements

Angle-of-attack measurements were made using a hot-wire anemometer with an X probe. The circuit used is shown in Figure 19. This arrangement was necessary because steady-state angles of attack were needed for the flow measurement. At a given tunnel speed, the hot wire was calibrated by rotating it through known angles. Tests were then conducted at the same tunnel speed and wire-heating currents.

C. Speed Measurements

A check was made of the influence of the bump upon the local wind speed in the vicinity of the wing trailing edge. With the bump in a forward position, there was a slight speed increase. This fell off

rapidly as the bump was moved back. A comparison made between the quasi-steady and dynamic speed effect showed no measurable difference. The measurement was made by using a hot wire mounted in the horizontal plane. A direct-current amplifier was used to amplify the effect of steady-state velocity changes.

D. Balance System

To measure the normal force on the test wing, a one component balance was designed and built. The primary sensing mechansim of the balance was used for measuring the force in both the 21- x 29-inch and 5- x 7-foot tunnels.

Two-dimensional flow was maintained across the wing by mounting end plates at each end of the model. A sketch of the end plates and test section for the 21- x 29-inch tunnel is shown in Figure 20. A similar arrangement was used in the 5- x 7-foot tunnel.

For the 21- x 29-inch tunnel tests, the wing was attached as a cantilever beam to the balance mechanism, which was bolted to one of the end plates. The system was designed so that, at a later date, three-dimensional tests could be made of the lift lag by removing the other end plate. A gap between the wing tip and the free end plate of 0.03 inch was maintained.

For the 5- x 7-foot tests, the same balance mechanism was used, but was mounted on different end plates. The wing size was increased from a 6-inch chord and 12-inch span to a 12-inch chord and 24-inch span. With the load increased by a factor of 4, the wing tip, which was formerly free, was restrained in lift and drag; moments were not taken out from this plate.

The balance system was mounted directly on the floor of the laboratory in order to reduce the vibration pickup caused by the noise of the bump rolling on its track. Rubber seals were placed where the system passed through the tunnel floor.

The root of the wing was rigidly attached to the lift plate. Three deflection beams tied the lift plate to the balance block, (see Figures 21 and 22). Deflection of the lift plate relative to the balance block was used to measure the normal force.

The arrangement of the deflection beams was such that the lift plate would deflect because of a lift force, or rotate about its flexural axis because of a pitching moment. Other force and moment components produced negligible deflection of the plate. The lift force was separated from the pitching moment by measuring the translation of the lift plate at its flexural axis. To measure this lift, the following mechanical system was used (see Figure 22b for a sketch and identification of components). The flexural axis of the balance is located at point A. A push rod having flexure hinges at each end coupled the lift plate to beam C. The flexure hinges were used to separate the rotational displacement from the translational displacement of the lift plate. Thus a deflection of the lift plate by a normal force would deflect beam C while a rotation of the lift plate from a pitching moment would cause no deflection of this beam. The beam C was coupled to the flexure system at B and its base was attached to the balance block. Beam C was rigid except where it was connected to the balance block. Motion at point A relative to the balance block was magnified by a factor of 4 at the tip of the beam where the core (D) of a Schaevitz transformer was mounted. Displacement of the transformer core changed the coupling in the transformer, and produced an electrical output proportional to the displacement and its direction. The detailed

exploded views of the balance block system are shown in Figure 21.

The wings used with the balance system were made of balsa wood. A series of ribs with balsa planking formed the structure. The cross-section was an NACA 0010 airfoil.

Checks were made on the dynamic response of the wing-balance combination. To measure the dynamic response, a known sinusoidal force was applied to the wing and the balance output was measured. The exciting force was applied by fitting a balsa glove about a given span station of the wing, and driving the glove by an M-B shaker, Model C-31. The push rod was connected to a galsa glove by a small beam which had two strain gauges attached to it. The strain gauges measured the input force, (see Figure 23 for details). The response of the wing-balance system for the 21- x 29-inch tunnel system is shown in Figure 24.

The electrical circuit used in conjunction with the Schaevitz transformer is given in Figure 25.

E. Recording Systems

To record the transient information, two sytems were used. The first, used in the 21- x 29-inch tunnel, was a dual beam oscilloscope, Du Mont model 202. The bump position was indicated by one trace and the balance response indicated by the other trace. Time was obtained by Z modulating the bump position beam. The information was recorded by photographing the oscilloscope face with Du Mont model 297 Polaroid-Land camera. The second system was a 14 channel recording oscillograph Consolidated model 5116 used to record the test data obtained in the 5- x 7-foot tunnel. With this unit, the time scale and response to bump position and lift force were considerably expanded. Typical traces for each of these techniques are given in Figure 26.

REFERENCES

1. Ashley, Zertarian, and Neilson, Investigation of Certain Unsteady Aerodynamic Effects in Longitudinal Dynamic Stability, USAF TR 5986.

2. Buchan, Harris, and Summervail, Measurements of Z_w for an Oscillating Airfoil, College of Aeronautics, Cranfield Report No. 40.

3. Bratt, J. B., and Scruton, C., Measurements of Pitching Moment Derivatives for an Airfoil Oscillating About the Half Chord Axis, Br ARC RAM, 1921.

4. Durand, W. F., Aerodynamic Theory. Durand Reprinting Committee, II.

5. Donely, P., An Experimental Investigation of the Normal Acceleration of an Airplane Model in a Gust. NACA TN 706, 1939.

6. Donely, P., Summary of Information Relating to Gust Loads on Airplanes, NACA TN 1976, 1949.

7. Farren, W. S., Reaction on a Wing Whose Angle of Incidence is Changing Rapidly, Br ARC R and M 1648, 1935.

8. Hakkinen, R. J., and Richardson, A. S., Jr., Theoretical and Experimental Investigation of Random Gust Loads. Part I—Aerodynamic Transfer Function of a Simple Wing Configuration in Incompressible Flow. NACA TN 3878, May 1957.

9. Halfman, R. L., Experimental Aerodynamic Derivatives of a Sinusoidally Oscillating Airfoil in Two-Dimensional Flow, NACA TN 2465, 1951.

10. Jones, R. T., Operational Treatment of the Nonuniform Lift Theory in Airplane Dynamics. NACA TN 667, 1938.

11. Karman, T. von, and Sears, W. R., "Airfoil Theory for Non-Uniform Motion," J. Aeronaut. Sci., Vol 10, August 1938.

12. Kuethe, A. M., Circulation Measurements About the Tip of an Airfoil During Flight Through a Gust. NACA TN 685, 1939.

REFERENCES (Concluded)

13. Kuethe, A. M., Schetzer, J. D., and Garby, L. C., Research Design Problems Relating to Facilities for Simulating the Aerodynamic Effects of Atmospheric Gusts on Aircraft Components, The University of Michigan, Engineering Research Institute Project 2099, Progress Report No. 4, 1953.

14. Kuethe, A. M., Schetzer, J. D., and Garby, L. C., Research Design Problems Relating to Facilities for Simulating the Aerodynamic Effects of Atmospheric Gusts on Aircraft Components, The University of Michigan, Engineering Research Institute Project 2099, Progress Report No. 5, 1954.

15. Milne-Thompson, L. M., Theoretical Aerodynamics. New York: D. Van Nostrand Company, 1947.

16. Wagner, H., "Dynamischer Auftrieb von Tragflügeln," Zeitschr. f. Angew. Math. u. Mech., Bd. 5, 1925.

17. Walker, P. B., Growth of Circulation About a Wing and Apparatus for Measuring Fluid Motion, Br ARC R and M 1402, 1931.

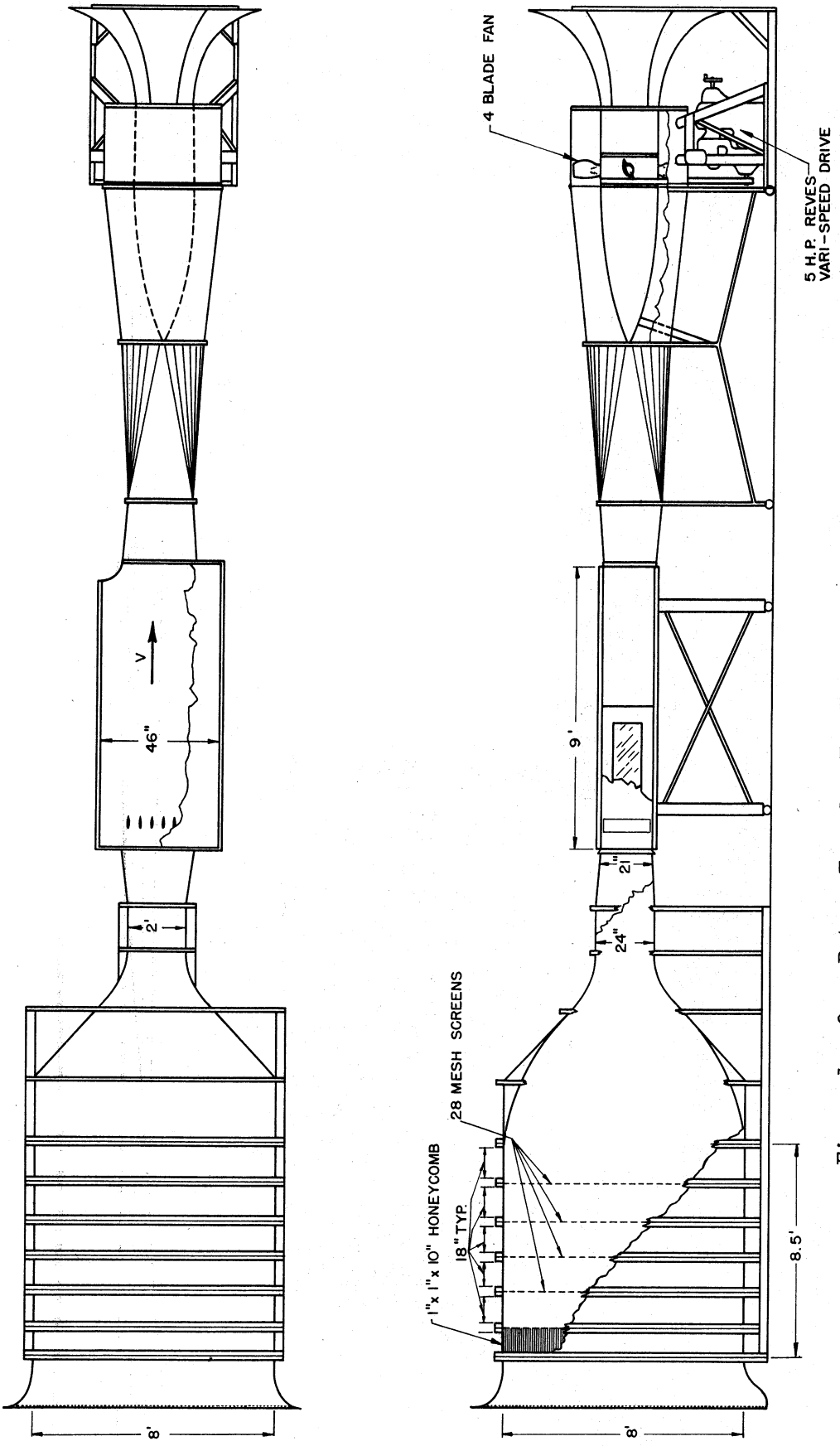

Figure 1. Open-Return Tunnel. The Vortex Gust Generator is Shown. The Moving Bump Gust Generator is Built Into Another Test Section Which is Interchangeable With the Above.

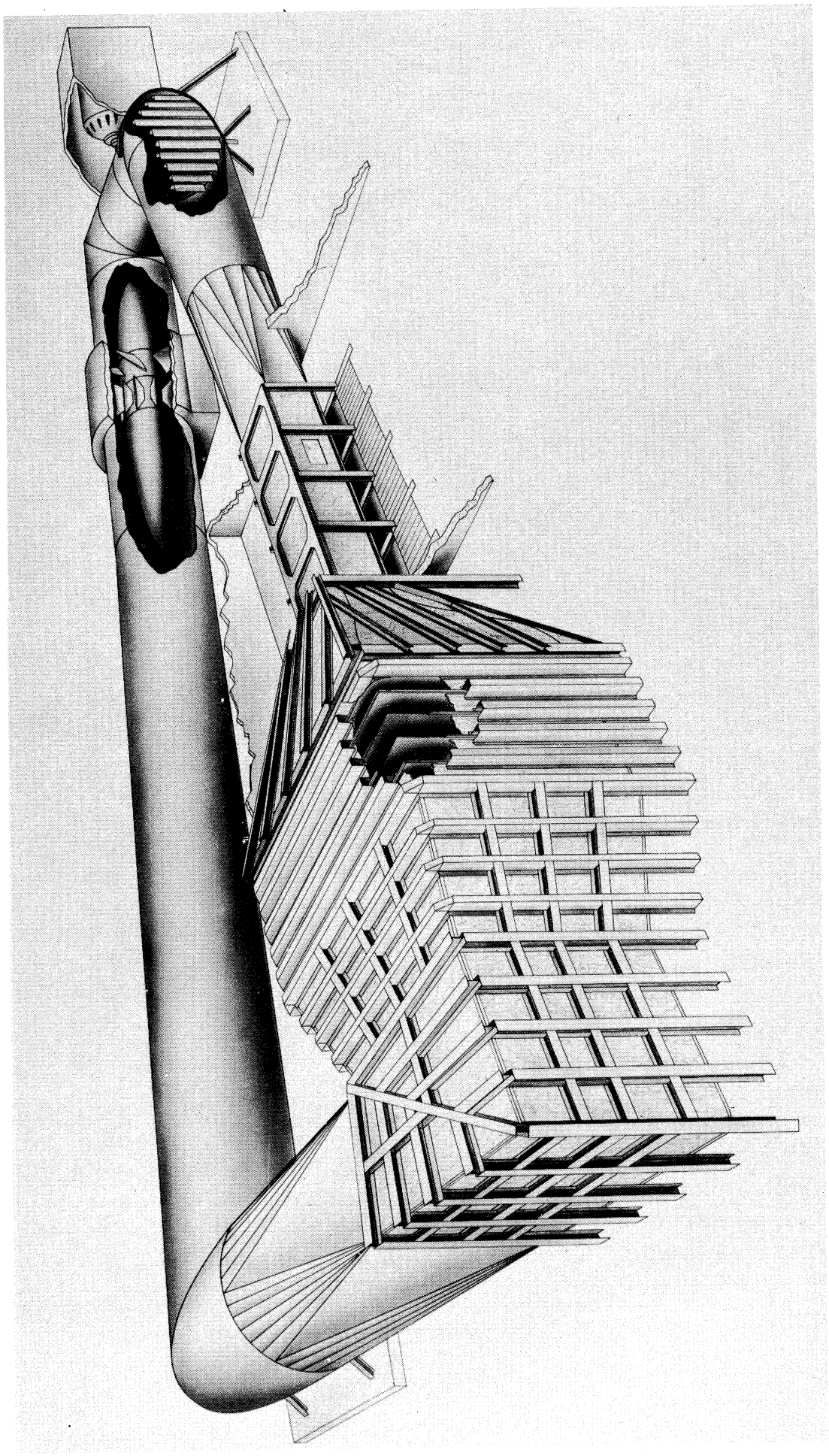

Figure 2-a. Perspective Drawing of 5 x 7 Feet Wind Tunnel

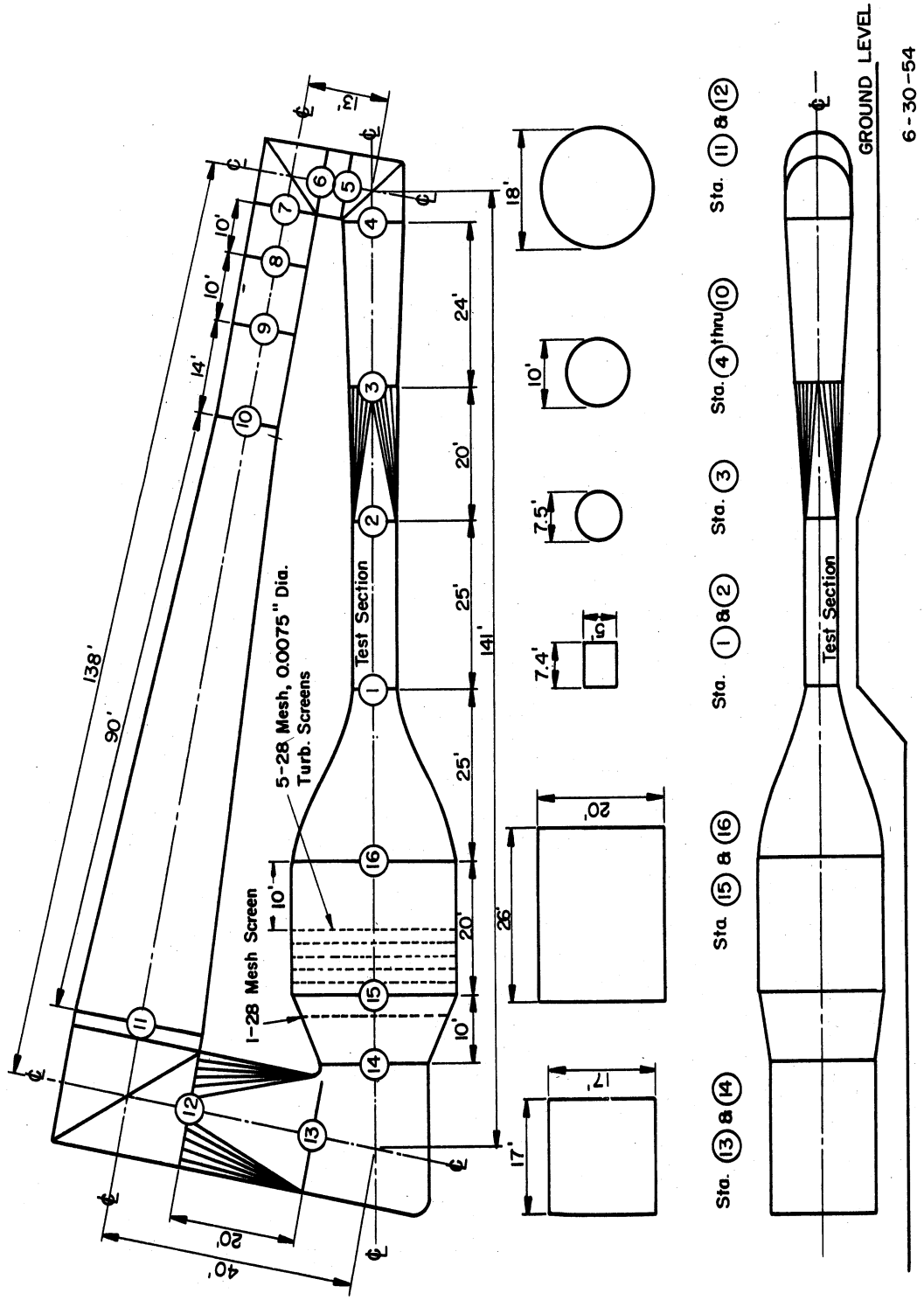

Figure 2-b. Plan View of 5 x 7 Foot Wind Tunnel.

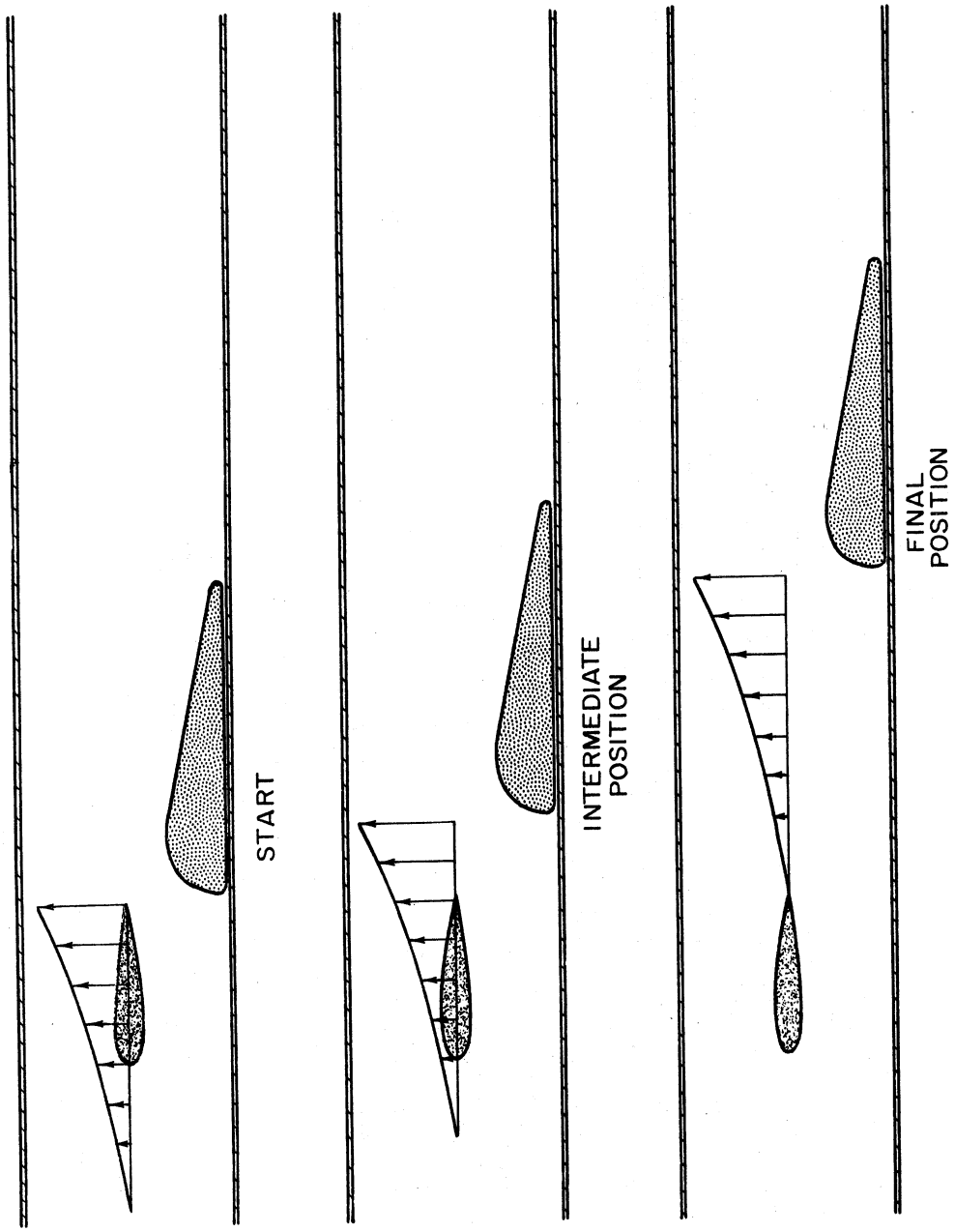

Figure 3. Normal Velocity Distribution for Three Positions of the Bump.

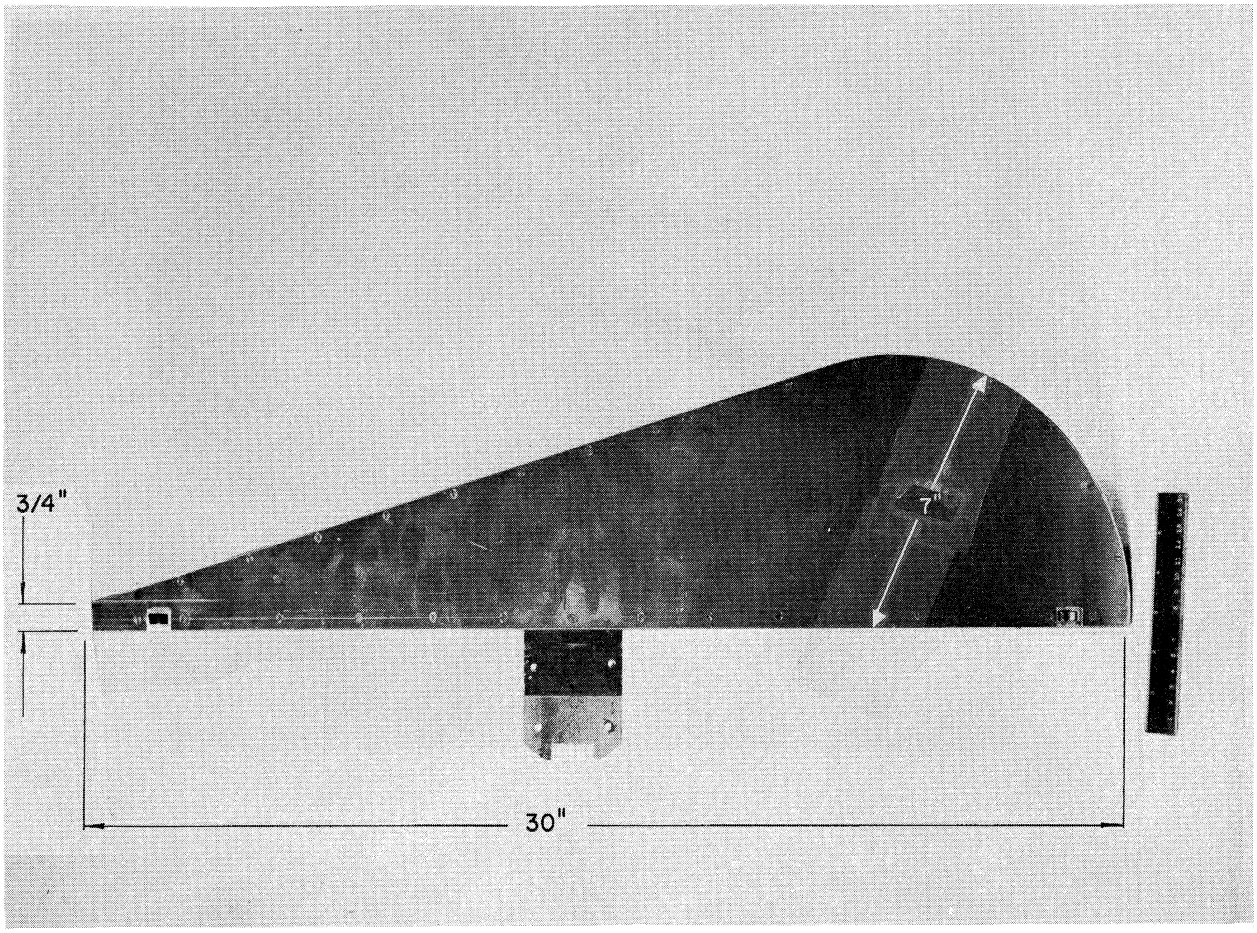

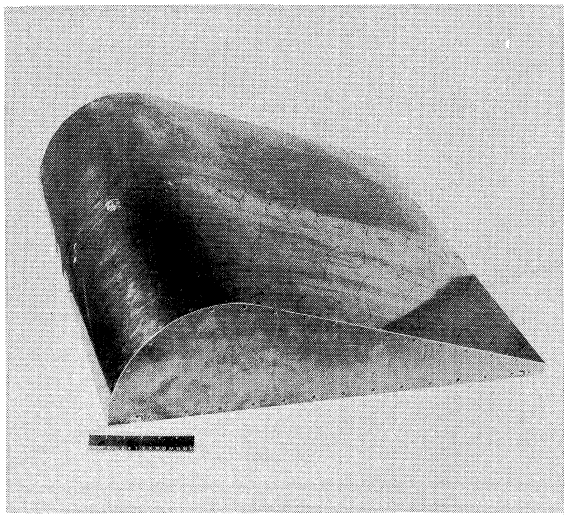

Figure 4-a. Photographs of Moving Bump and its Dimensions as Used In 21 x 29 Inch Open-Return Tunnel.

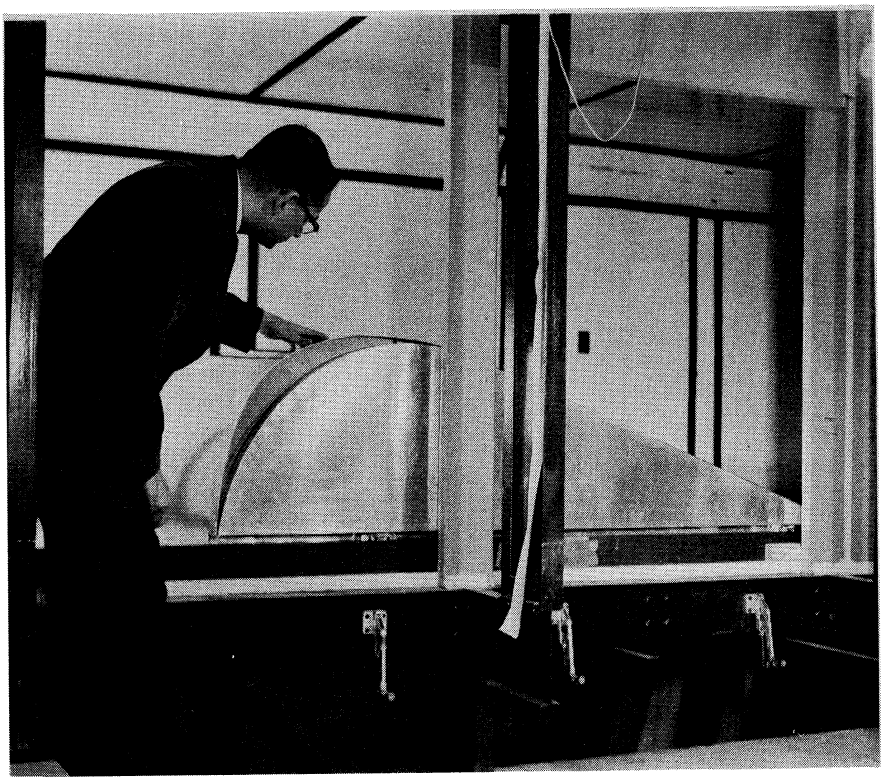

Figure 4-b. Photograph of Moving Bump in 5 x 7 Foot Tunnel.

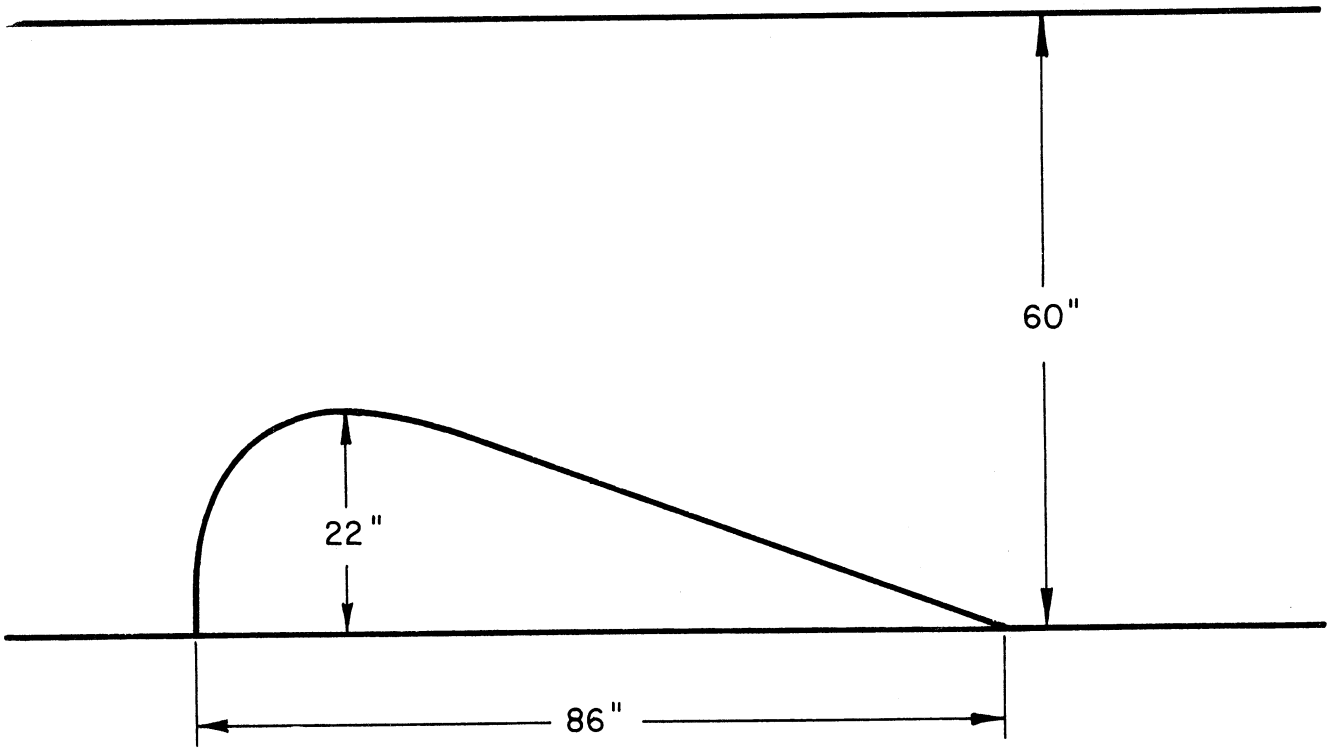

Figure 4-c. Sketch of Moving Bump in 5 x 7 Foot Tunnel.

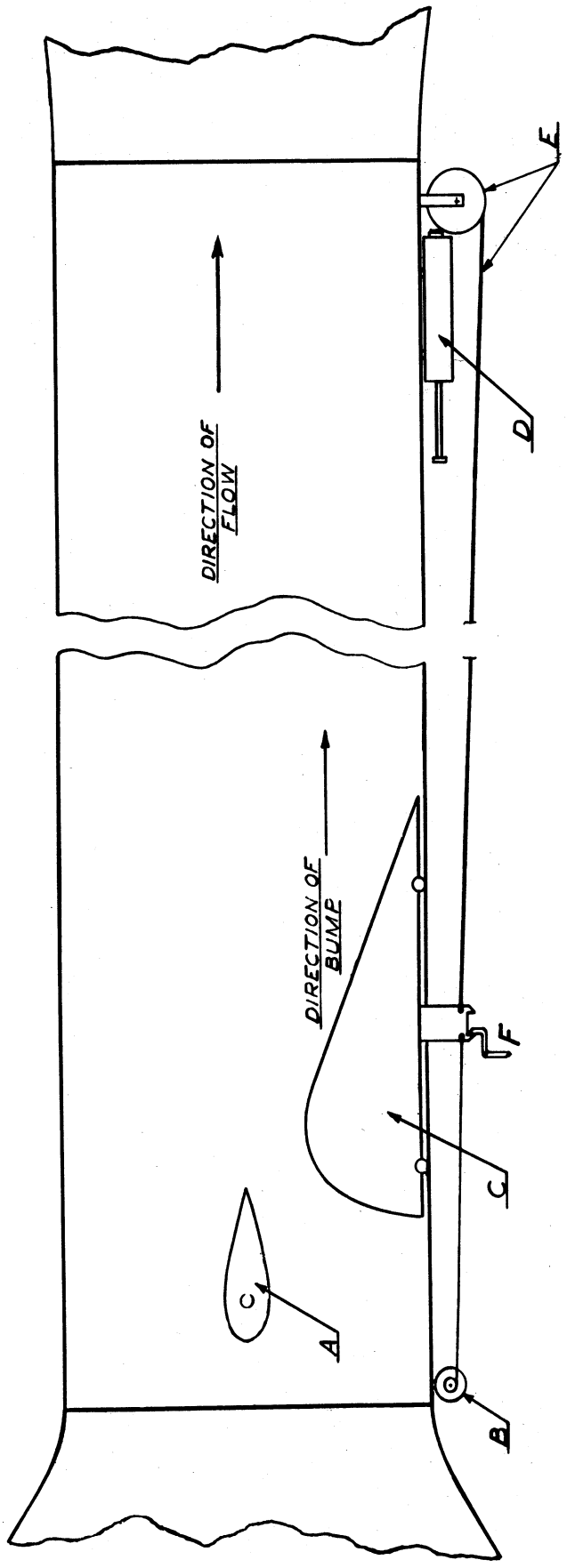

A. Test model.
B. Potentiometer to determine position of bump.
C. Moving bump.
D. Shock absorbing cylinder.
E. Accelerating mechanism (aircraft shock cord & winding drum).
F. Latch

Figure 5. Schematic Diagram of Moving Bump Gust Generator.

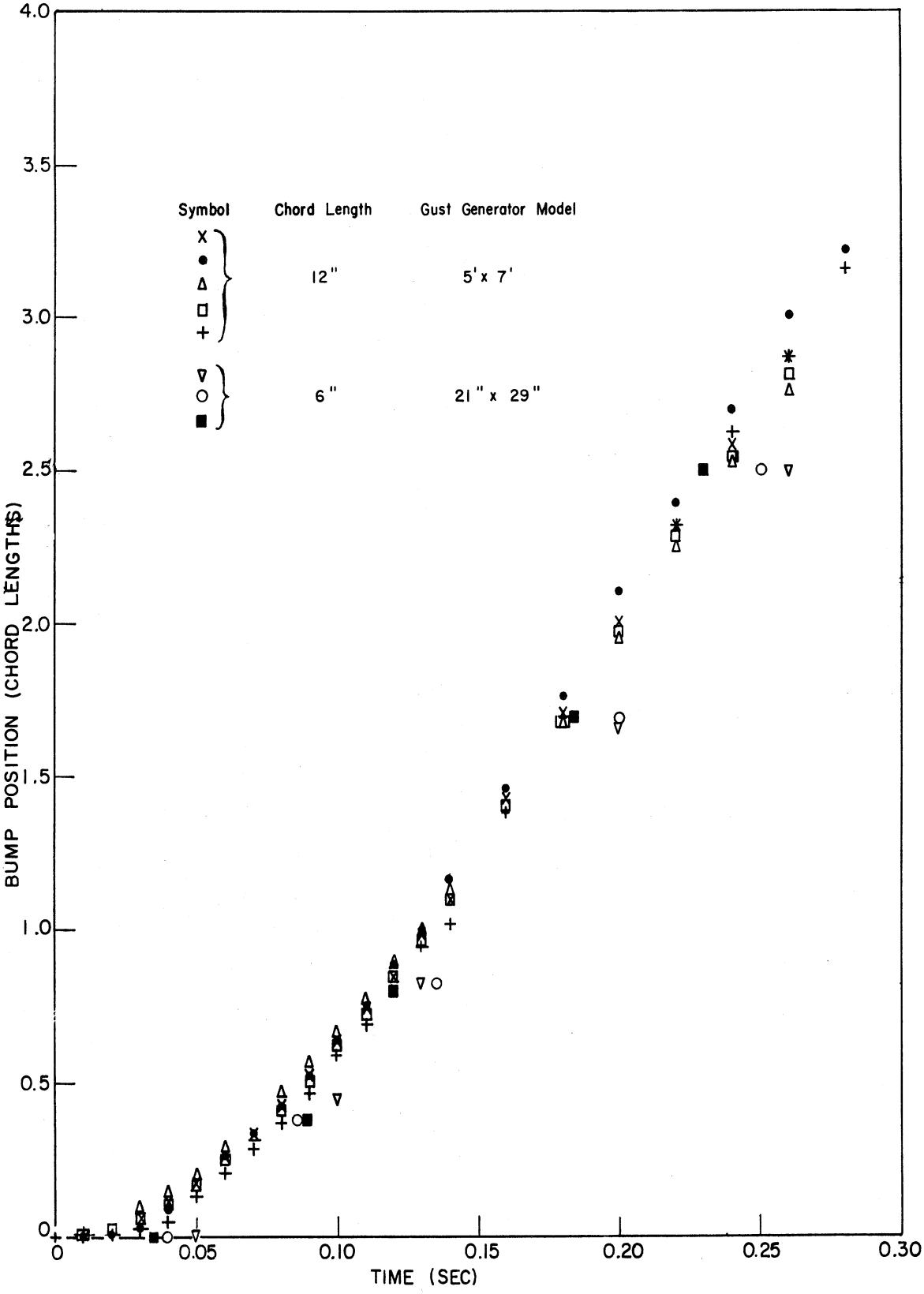

Figure 6. Bump Position in Chord Lengths vs. Time.

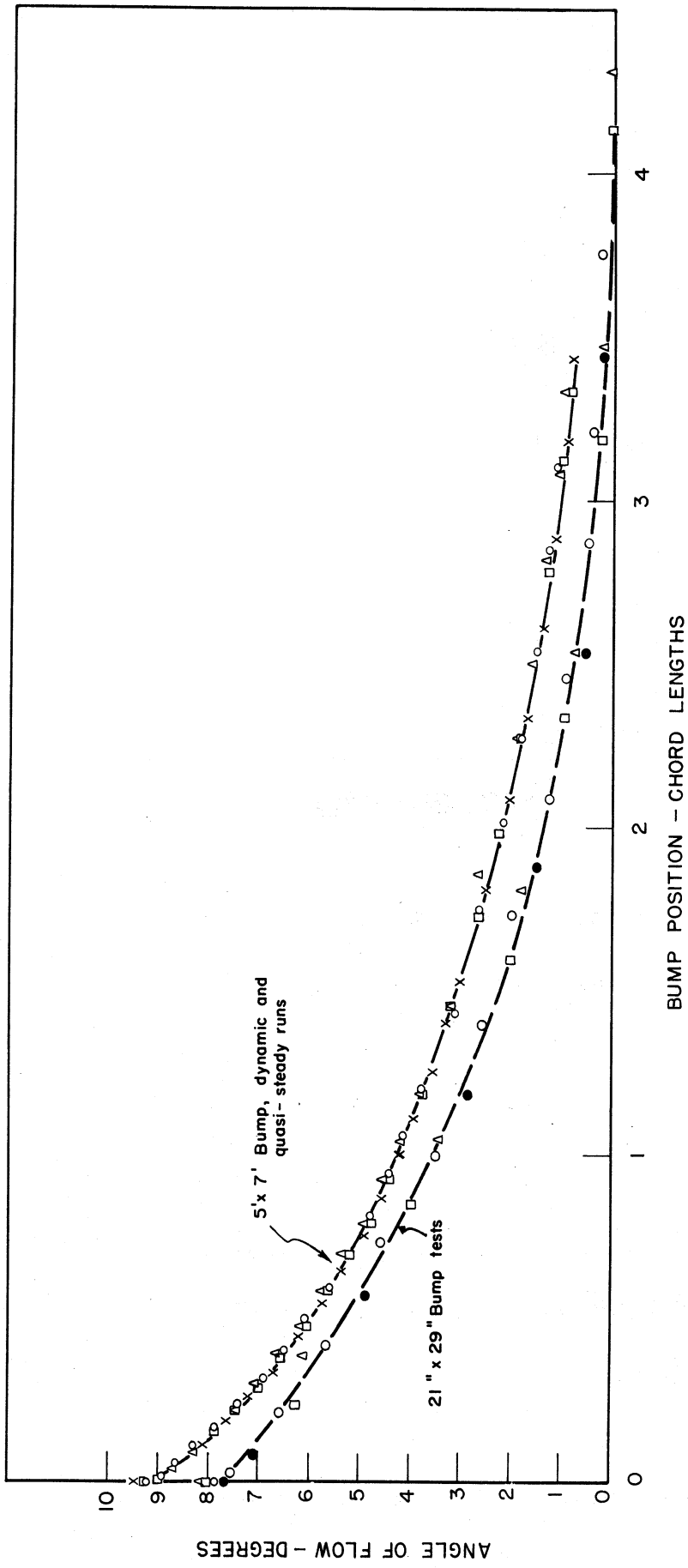

Figure 7. Flow Inclination in Degrees vs. Bump Position in Wing Chords..

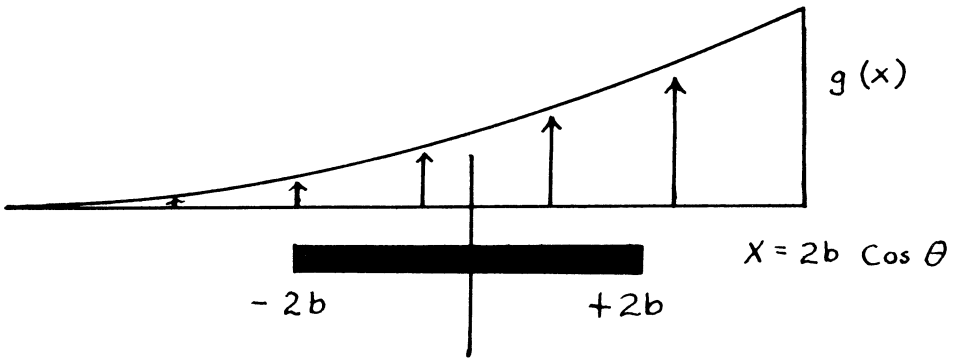

a. Model of the Gust Input

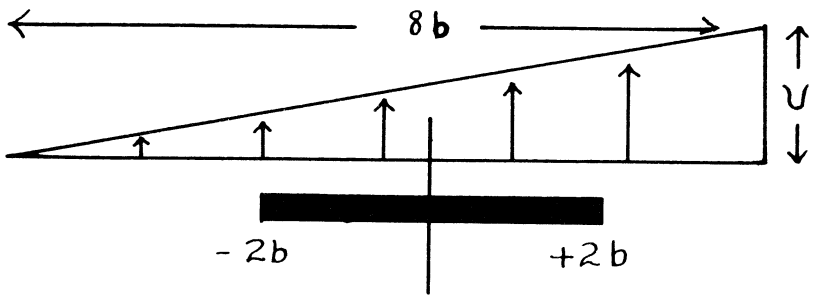

b. Model of Gust Input Used to Calculate L_a'

Figure 8. Models of the Gust Input.

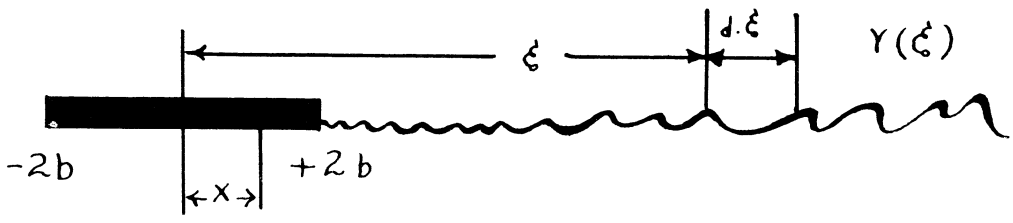

Figure 9. Model of the Wake Vortex Sheet

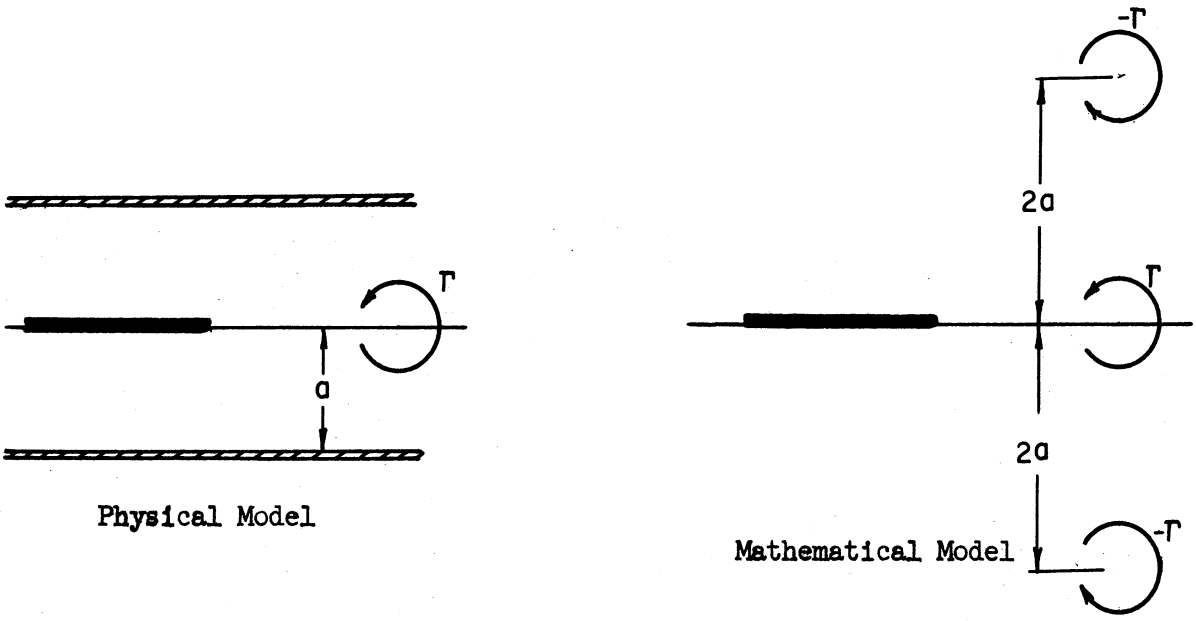

Figure 10. Sketch Showing Physical and Corresponding Mathematical Model of Wing and Wake Vortex Systems.

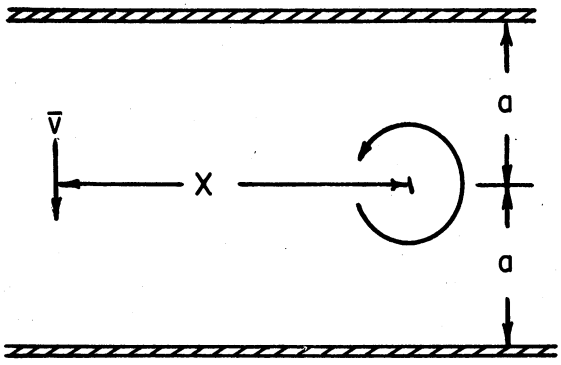

Figure 11. Sketch of Model Used to Calculate Attenuating Effect of Tunnel Walls Upon $\bar{v}$.

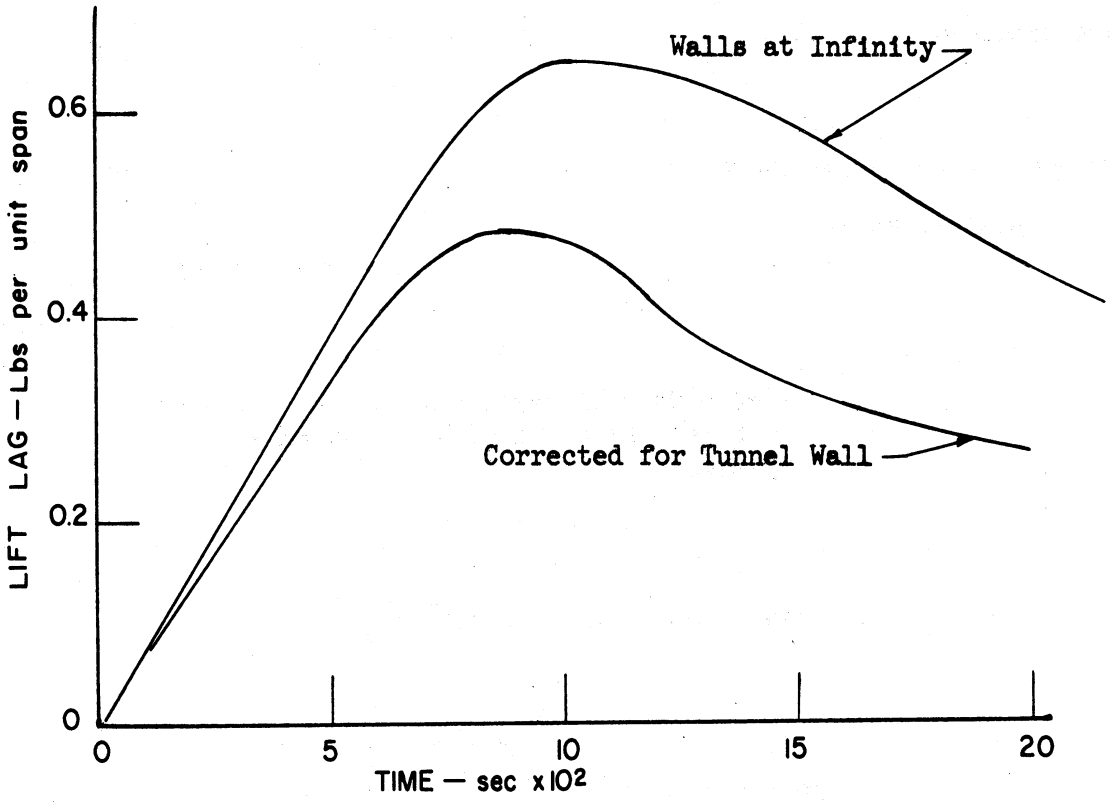

Figure 12. Comparison of Theoretical Lift Lag with the Tunnel Wall Correction and without Tunnel Wall Correction. 5 x 7 Foot Tunnel, V = 72.5 fps, Bump Speed = 14.3 fps.

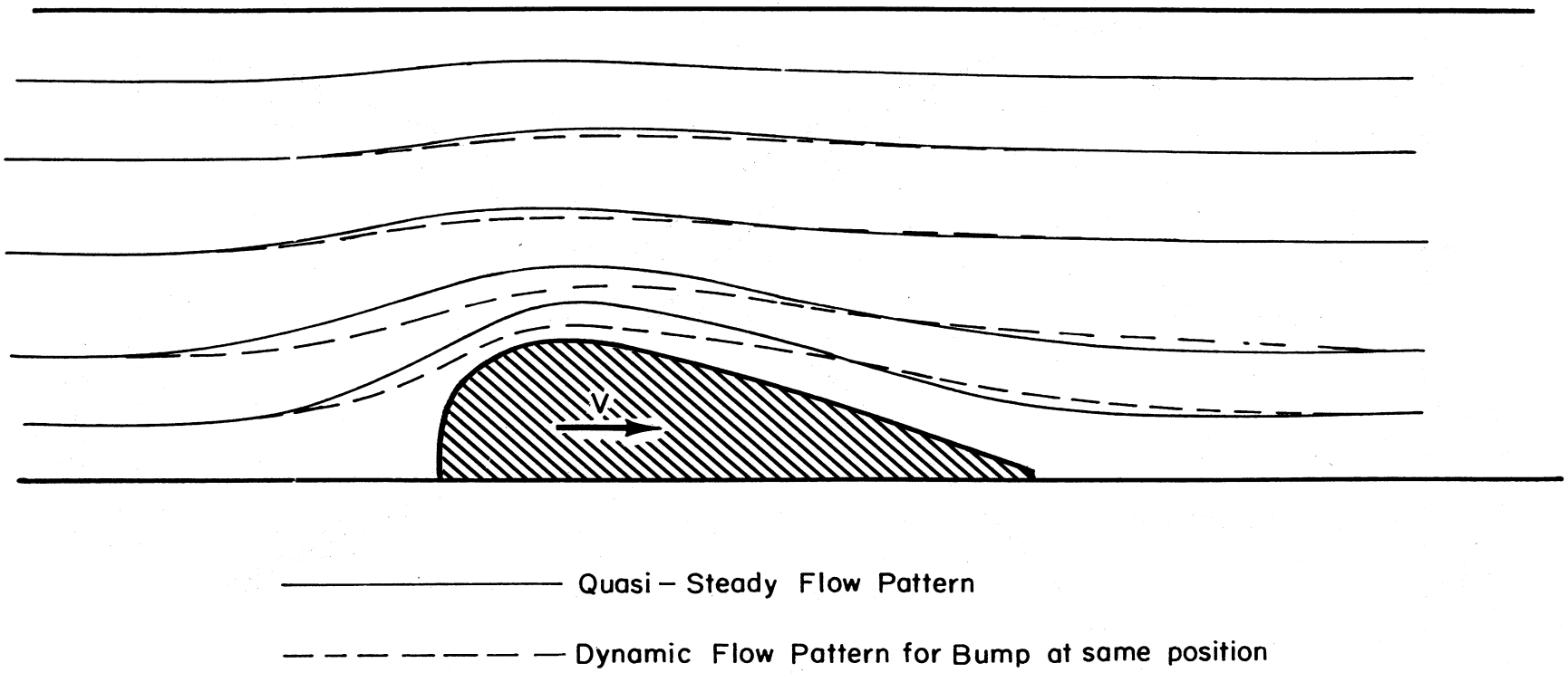

Figure 13. Quantitative effect of bump position upon flow-streamline distribution.

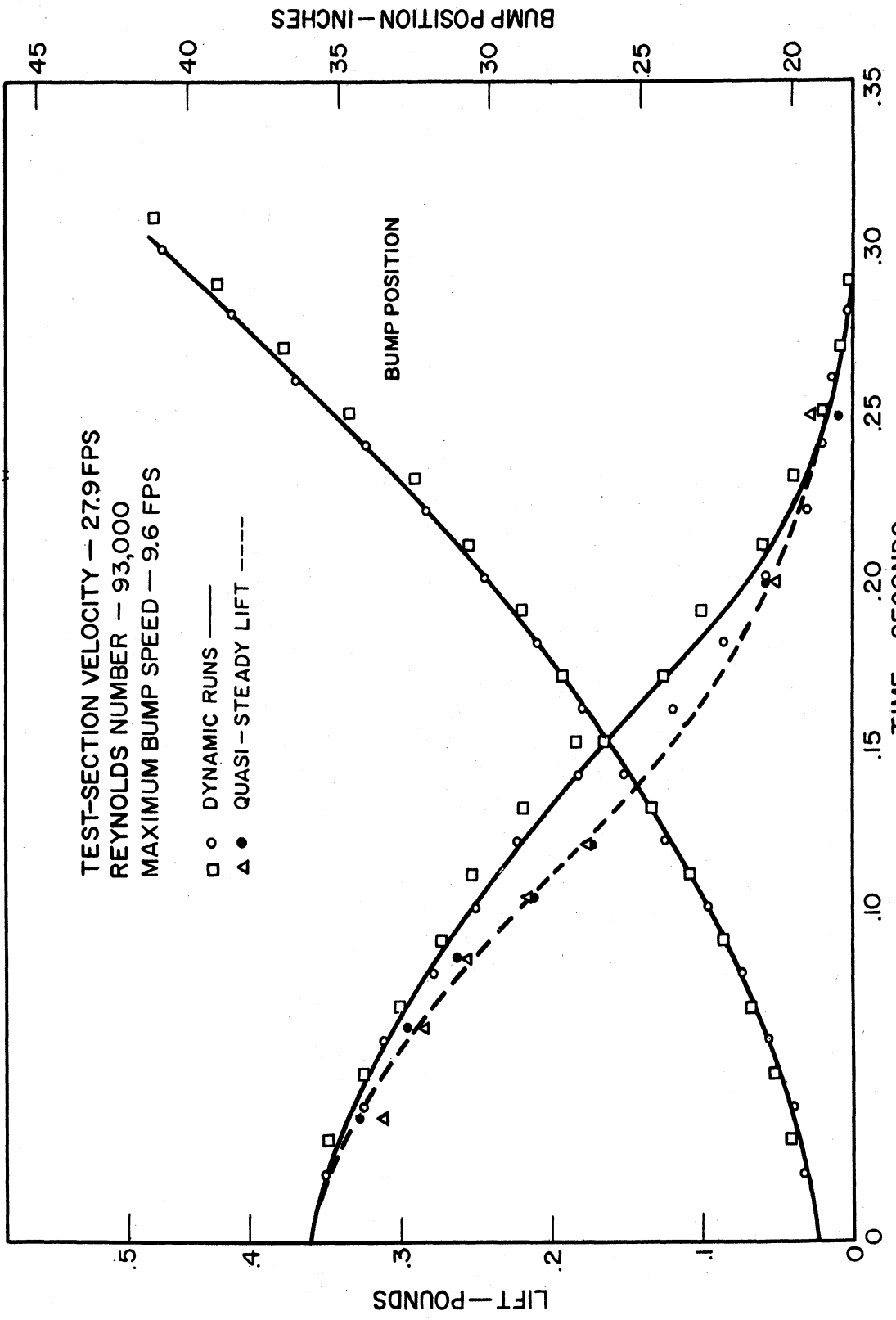

Figure 14-a. Measured Dynamic Lift, Quasi-Steady Lift, and Bump Position vs. Time for Test-Section Velocity of 27.9 fps.

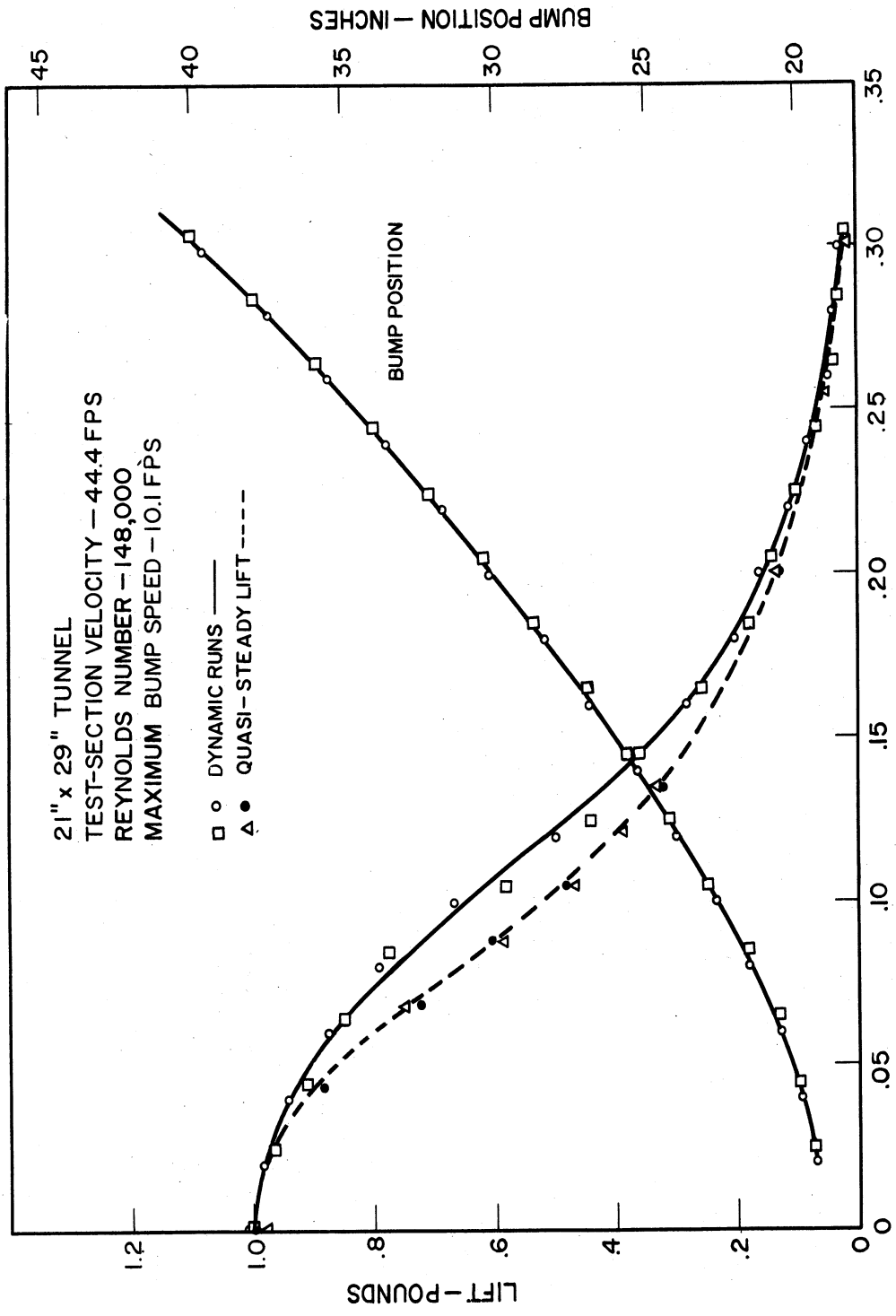

Figure 14-b. Measured Dynamic Lift Quasi-Steady Lift, and Bump Position vs. Time for a Test-Section Velocity of 44.4 fps

21 x 29 Inch Tunnel

Tunnel Speed 27.9 fps

Bump Speed 9.6 fps

Reynolds No. 93,000

Wing 12" Span
6" Chord

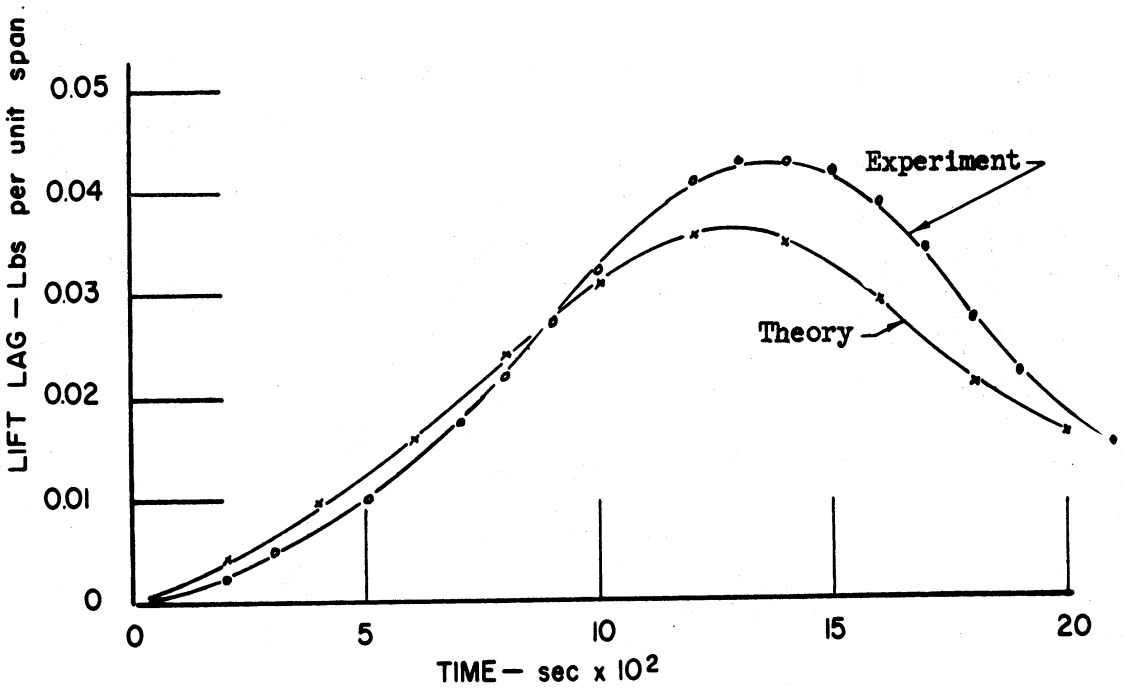

Figure 15-a. Comparison of Experimental and Theoretical Lift Lag Results. 21 x 29 Inch Tunnel

21 x 29 Inch Tunnel

Tunnel Speed 44.4 fps

Bump Speed 10.1 fps

Reynolds No. 148,000

Wing 12" Span
6" Chord

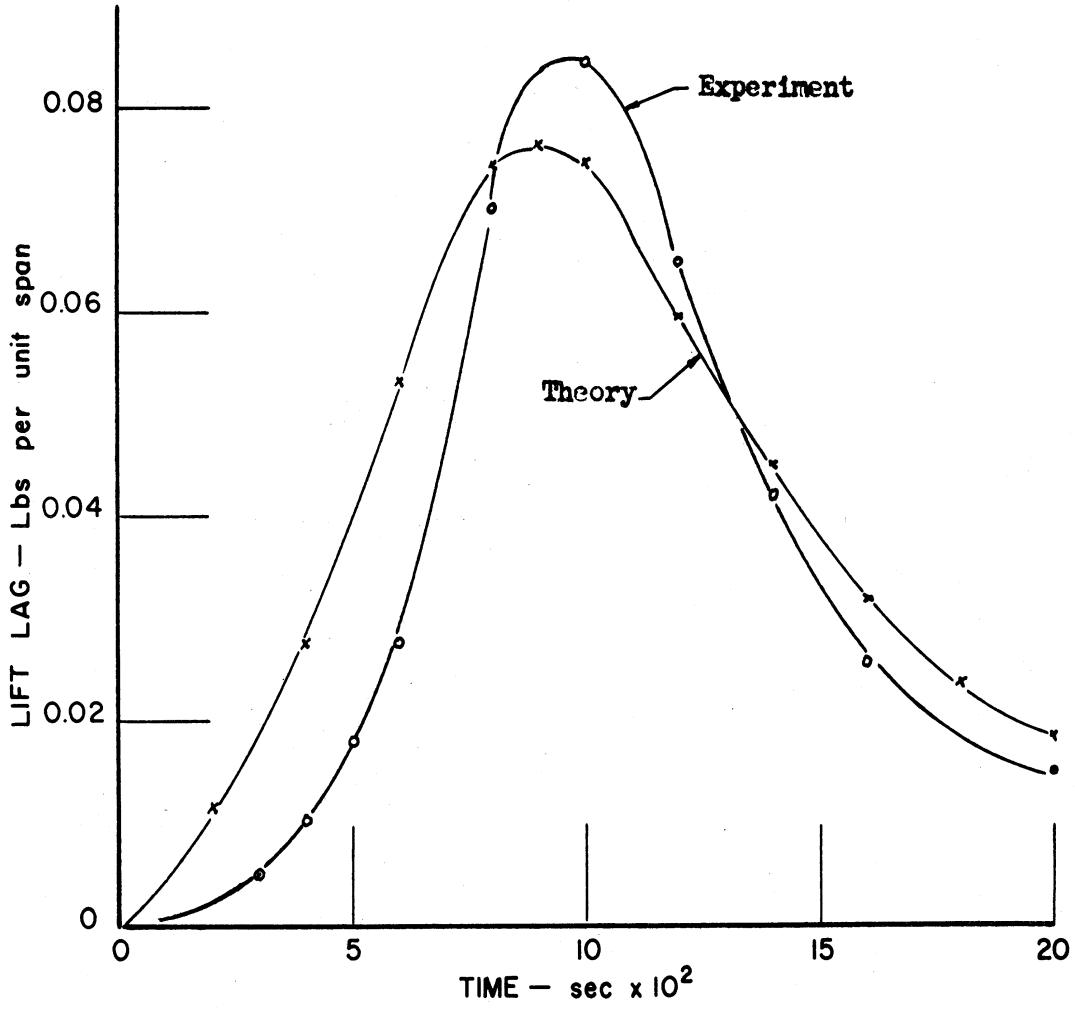

Figure 15-b. Comparison of Experimental and Theoretical Lift Lag Results. 21 x 29 Inch Tunnel.

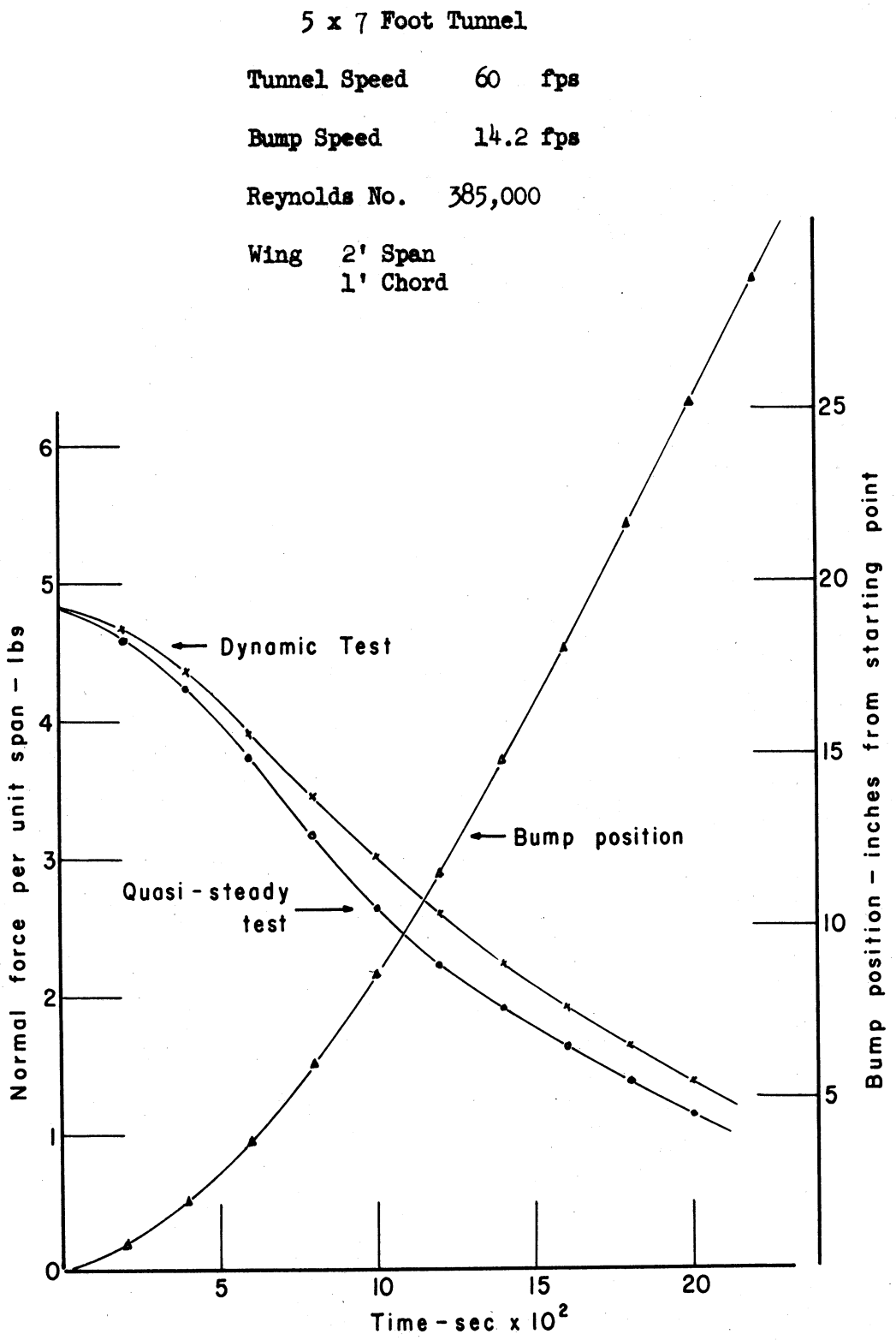

Figure 16-a. Quasi-Steady and Dynamic Normal Force Response and Bump Position Plotted as a Function of Time. 5 x 7 Foot Tunnel.

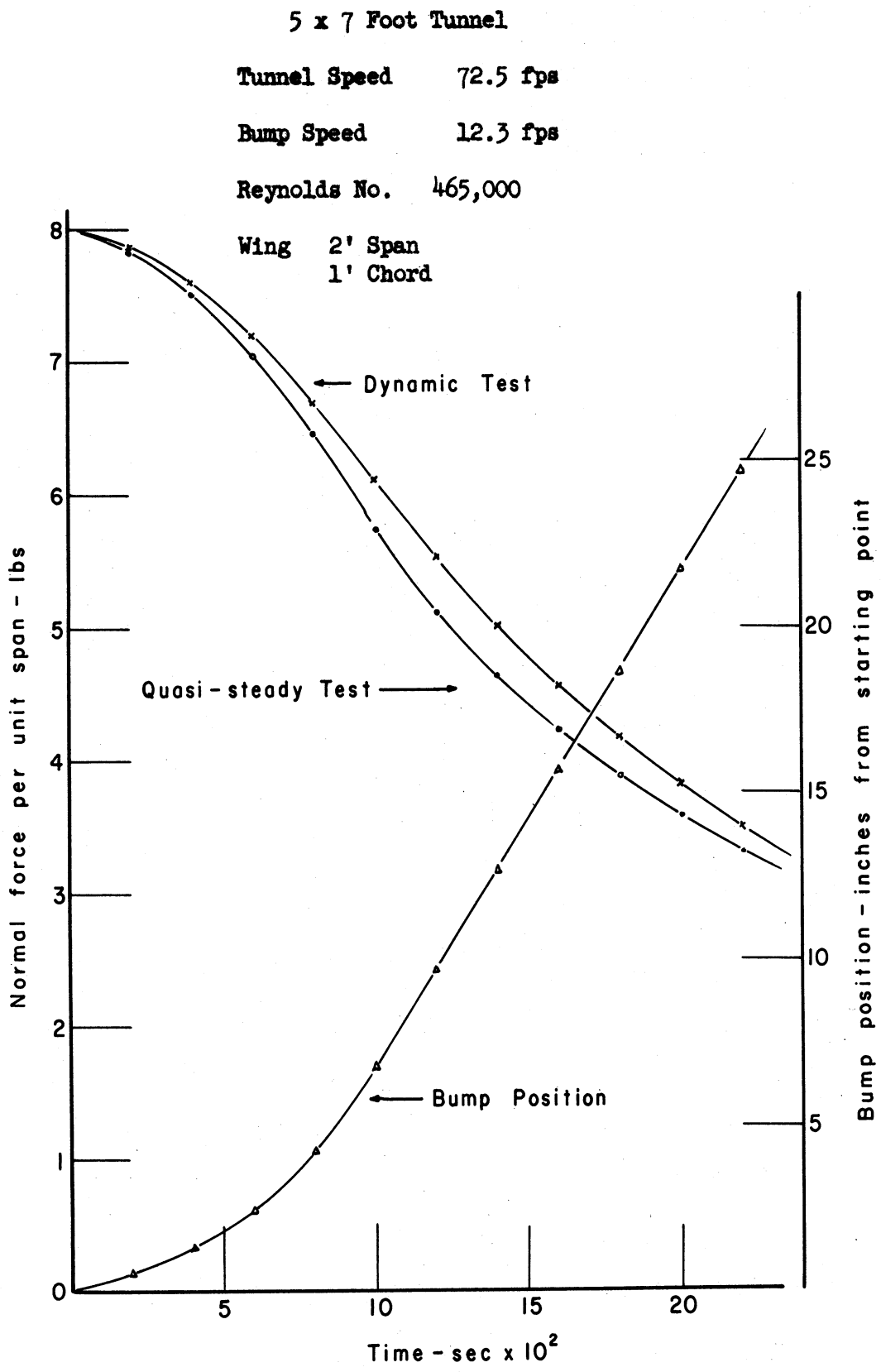

Figure 16-b. Quasi-Steady and Dynamic Normal Force Response and Bump Position Plotted as a Function of Time. 5 x 7 Foot Tunnel.

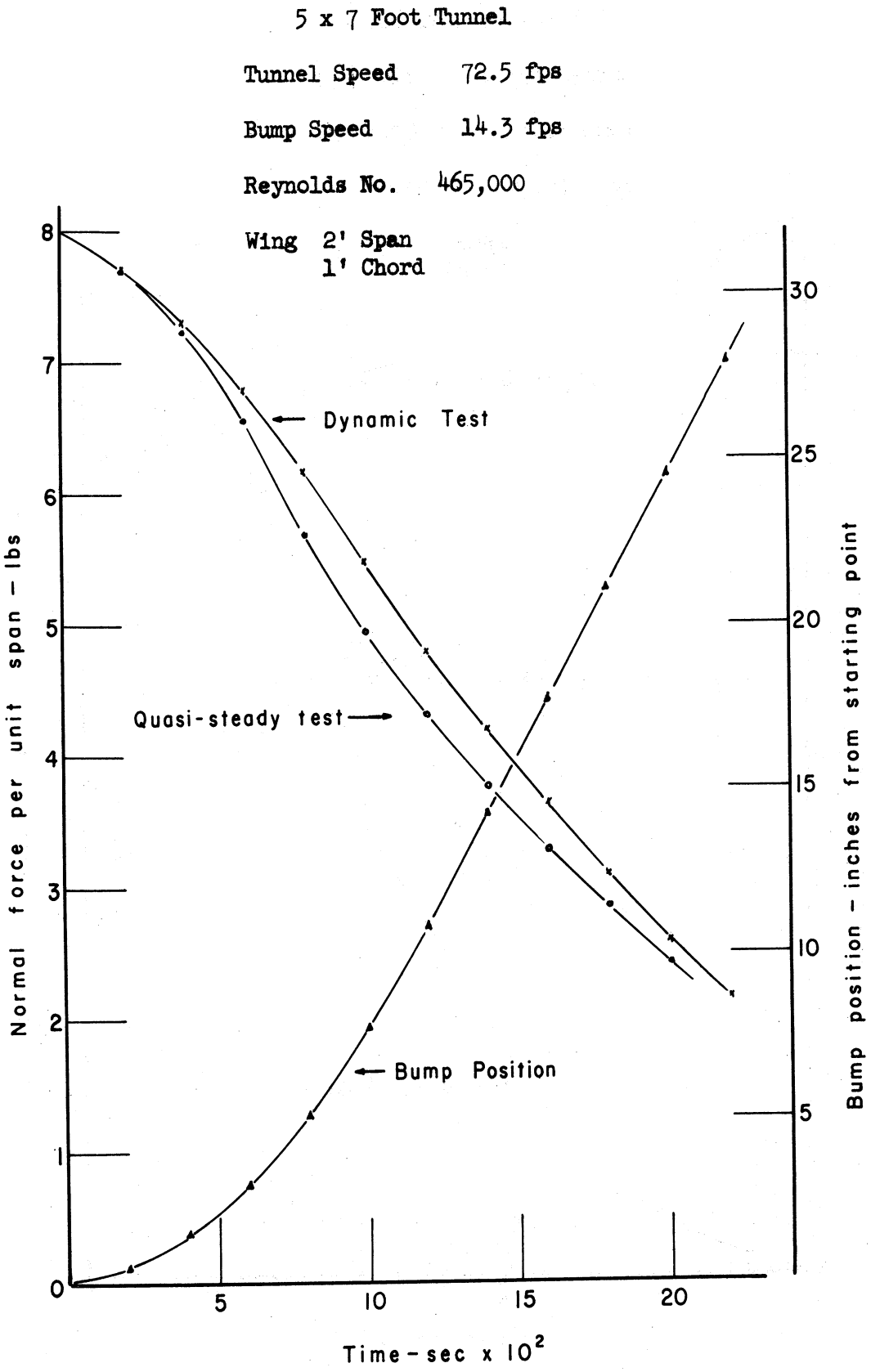

Figure 16-c. Quasi-Steady and Dynamic Normal Force Response and Bump Position plotted as a Function of Time. 5 x 7 Foot Tunnel.

5 x 7 Foot Tunnel

Tunnel Speed 60 fps

Bump Speed 14.2 fps

Reynolds No. 385,000

Wing 2' Span
1' Chord

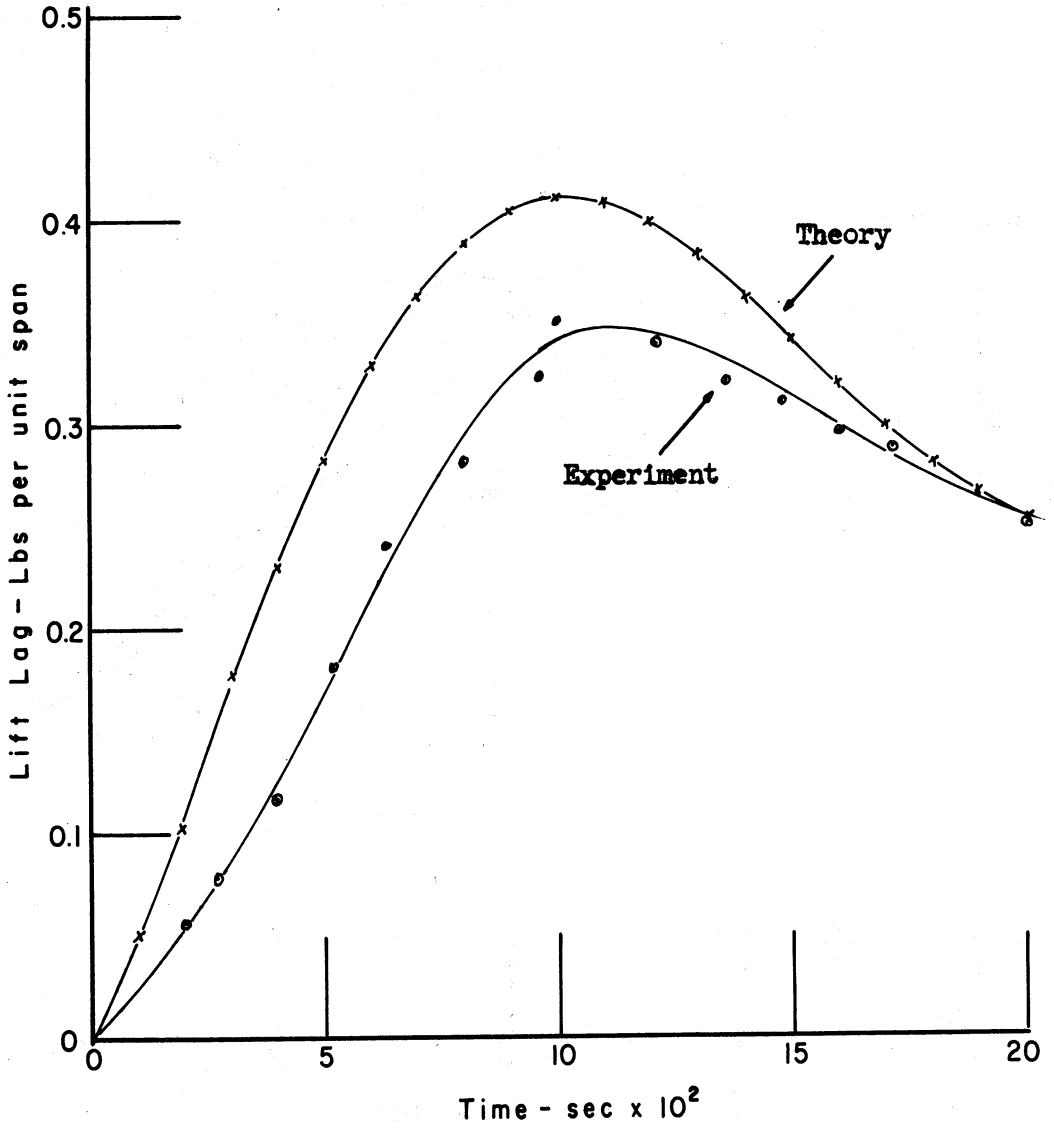

Figure 17-a. Comparison of Experimental and Theoretical Lift Lag Results. 5 x 7 Foot Tunnel.

5 x 7 Foot Tunnel

Tunnel Speed 72.5 fps

Bump Speed 12.3 fps

Reynolds No. 465,000

Wing 2' Span
1' Chord

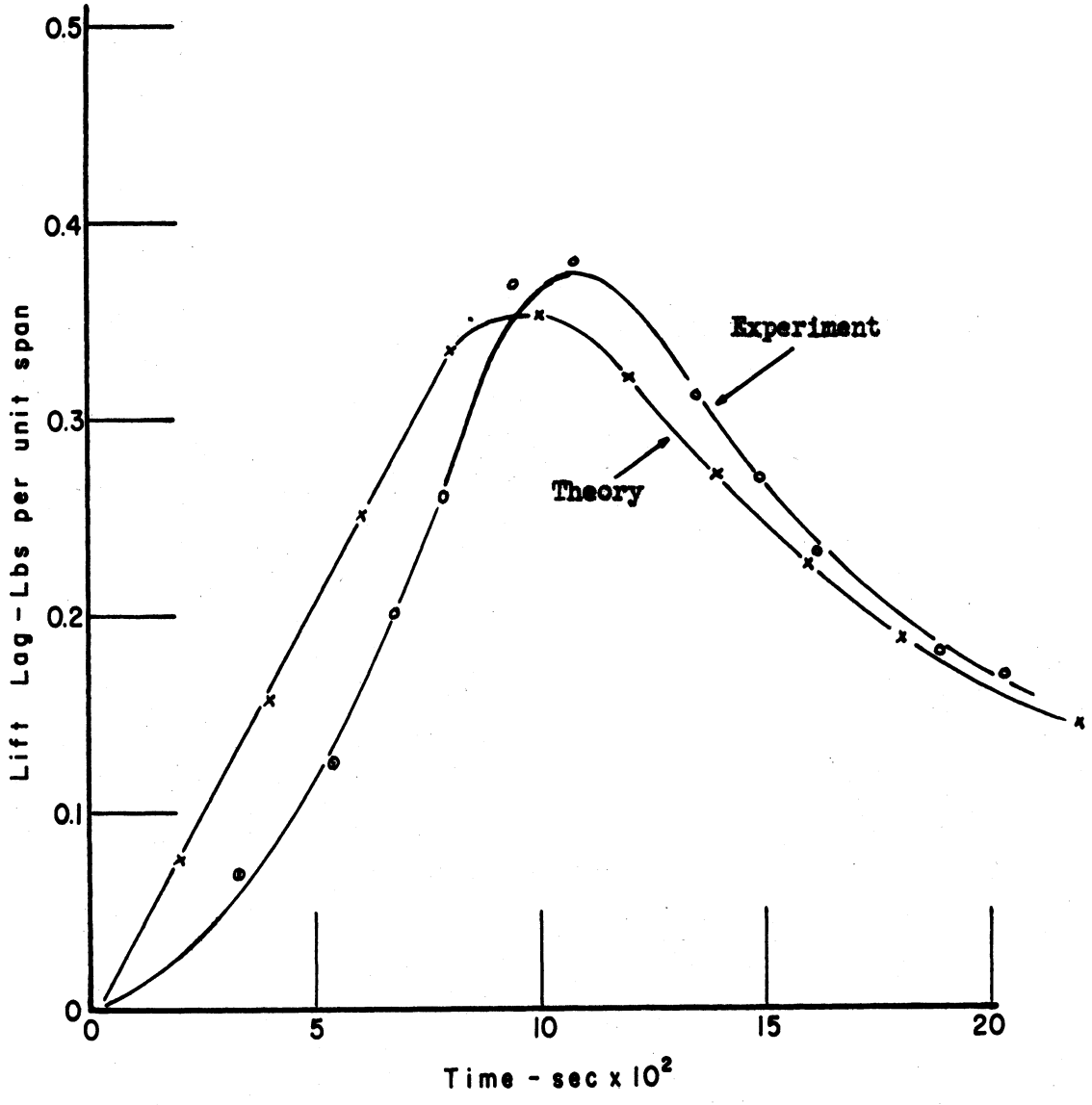

Figure 17-b. Comparison of Experimental and Theoretical Lift Lag Results. 5 x 7 Foot Tunnel.

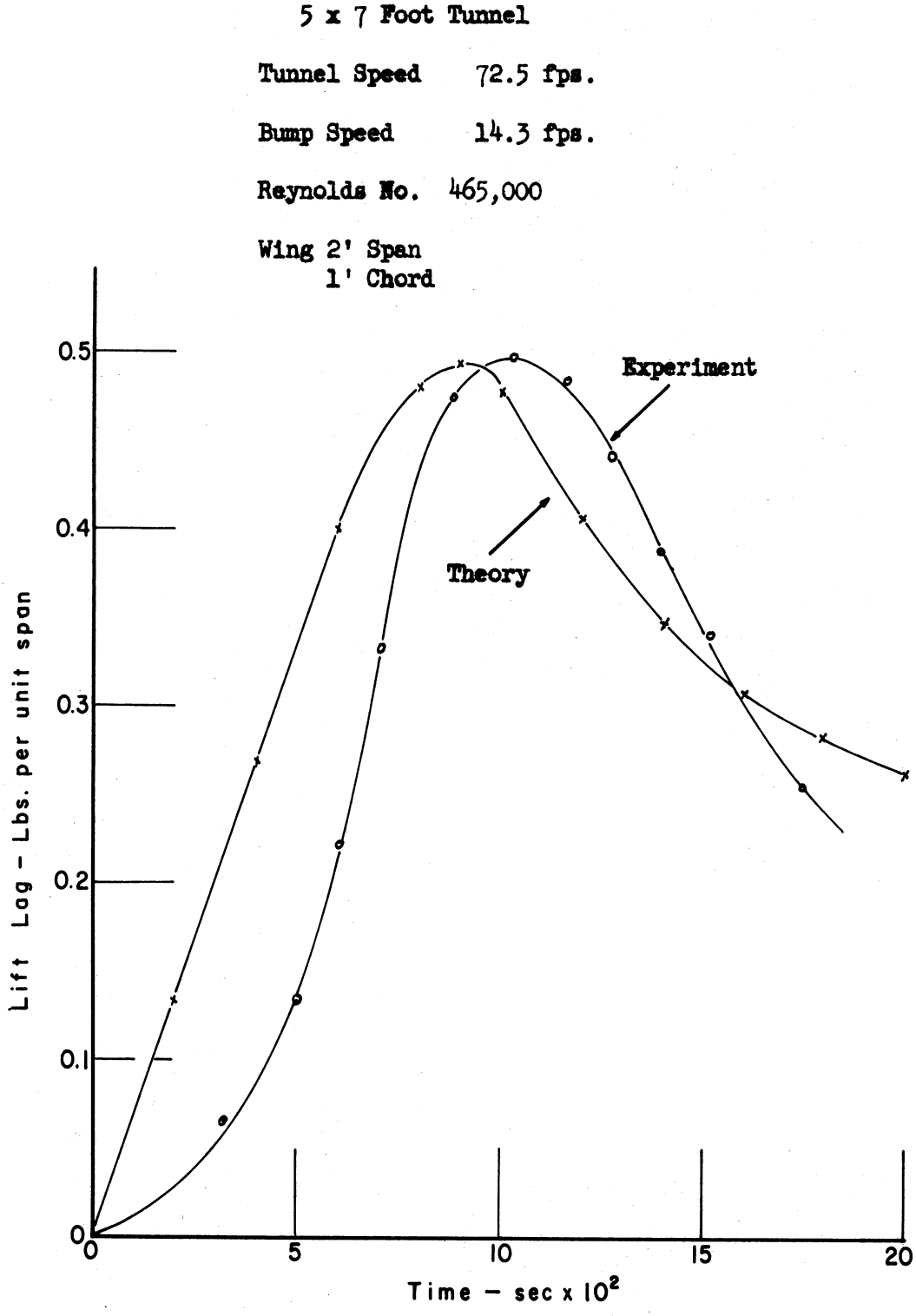

Figure 17-c. Comparison of Experimental and Theoretical Lift Lag Results. 5 x 7 Foot Tunnel.

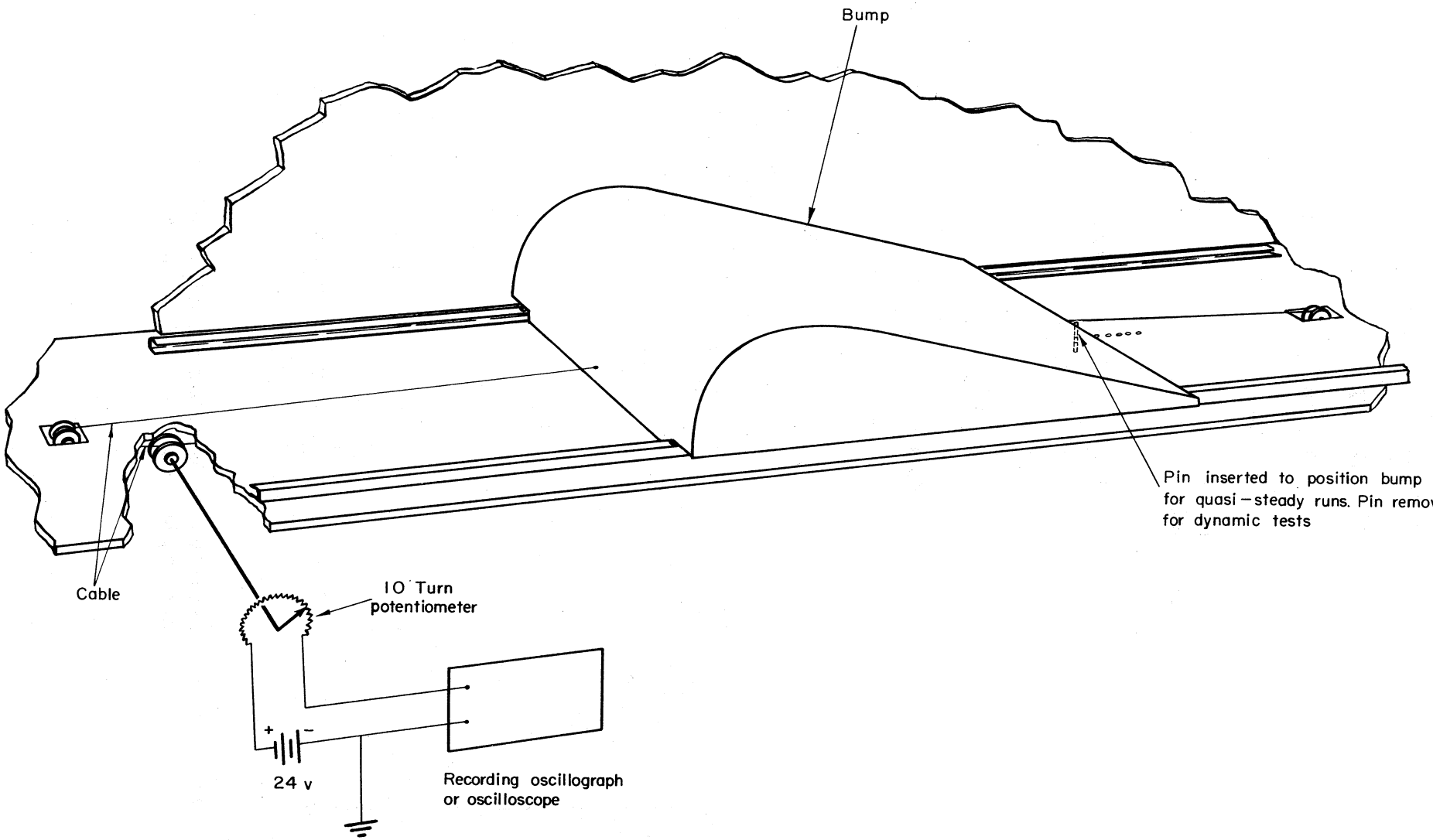

Figure 18. Sketch of Bump-Position Mechanism.

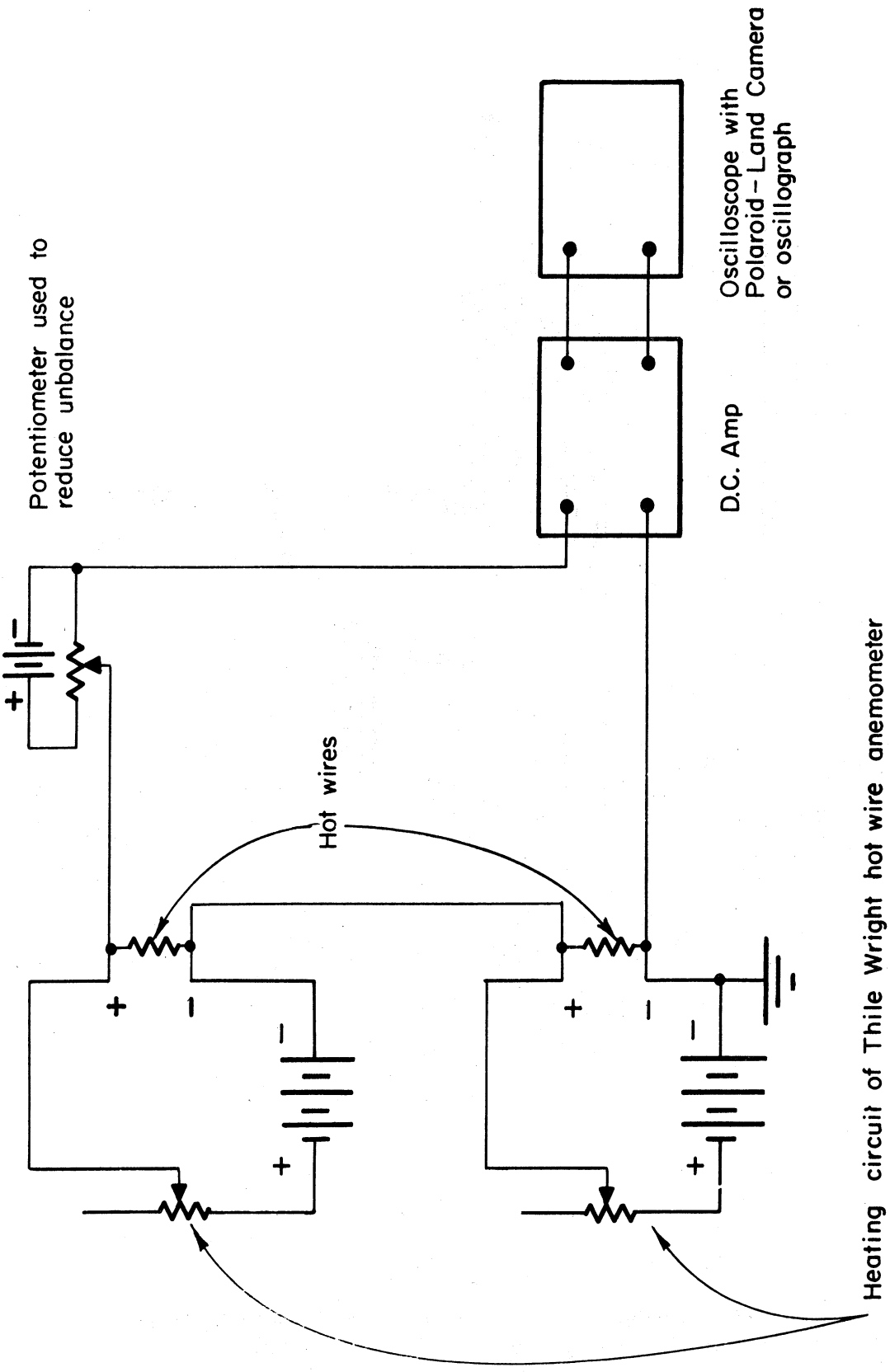

Figure 19. Electrical Circuit Used to Measure Flow Angles.

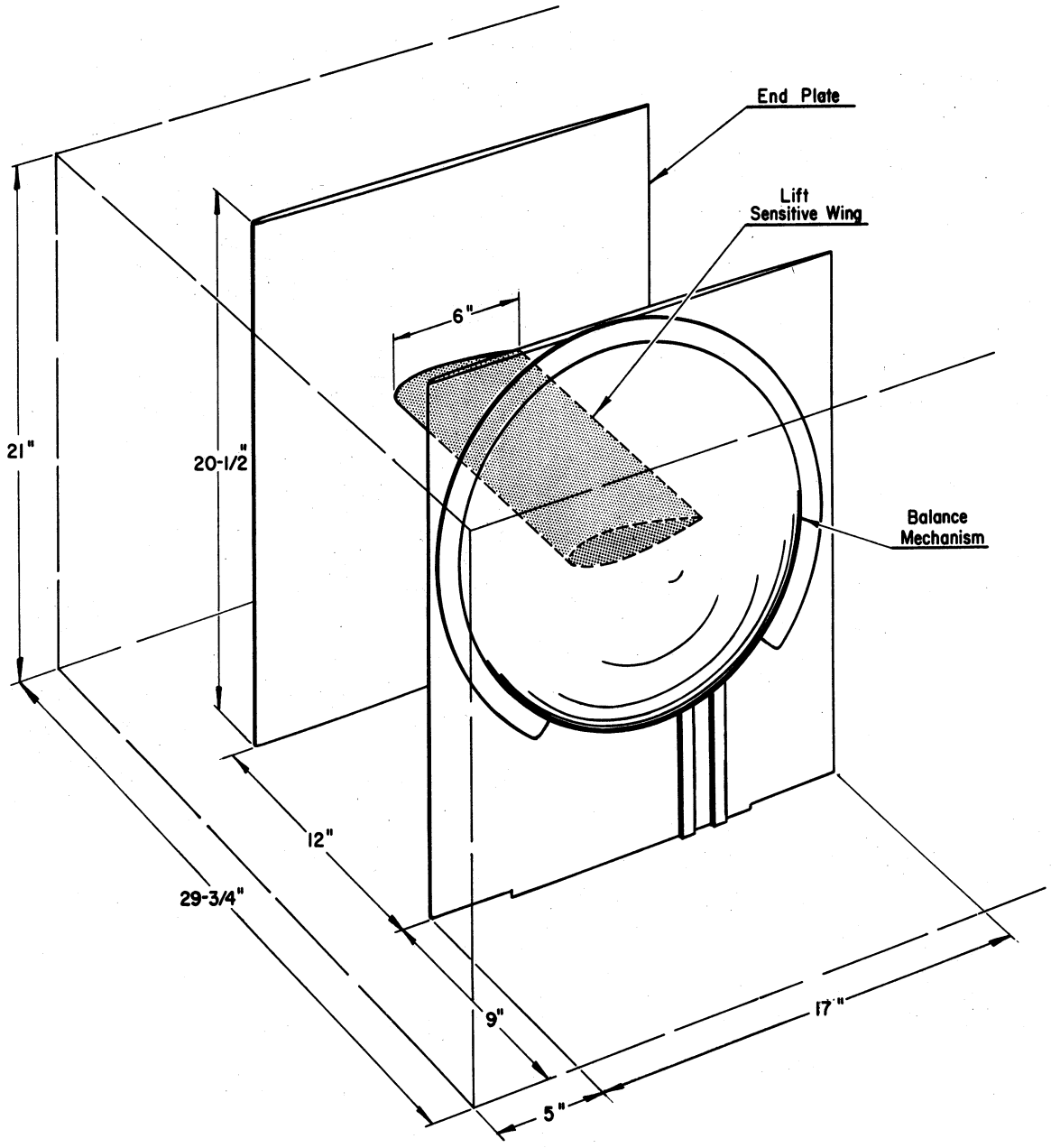

Figure 20. Sketch of General Arrangement of Lift Sensitive Wing and End Plates in the 21 x 29 Inch Tunnel.

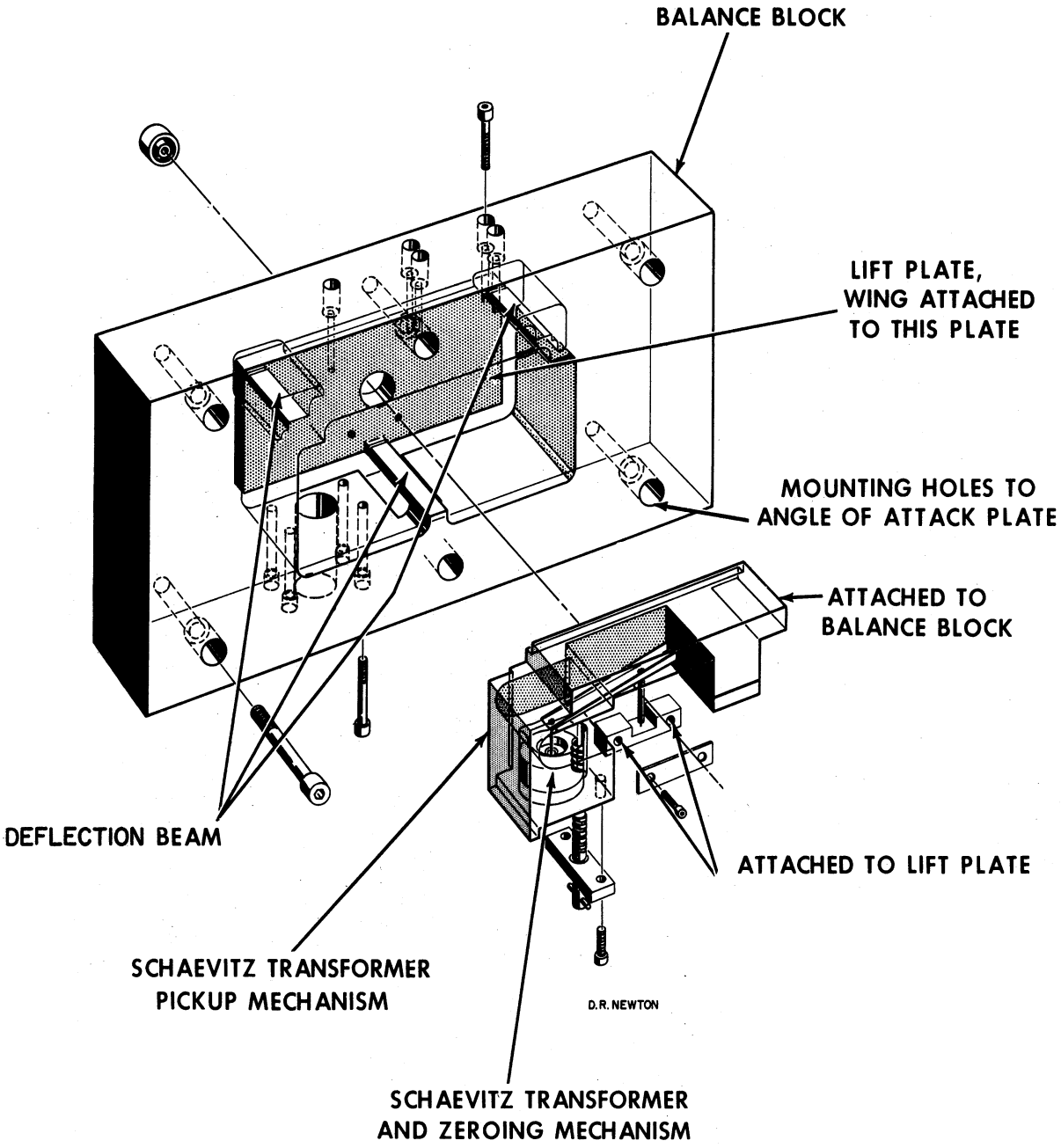

Figure 21. View Showing Deflection-Beam Block and Schaevitz Transformer Mounting.

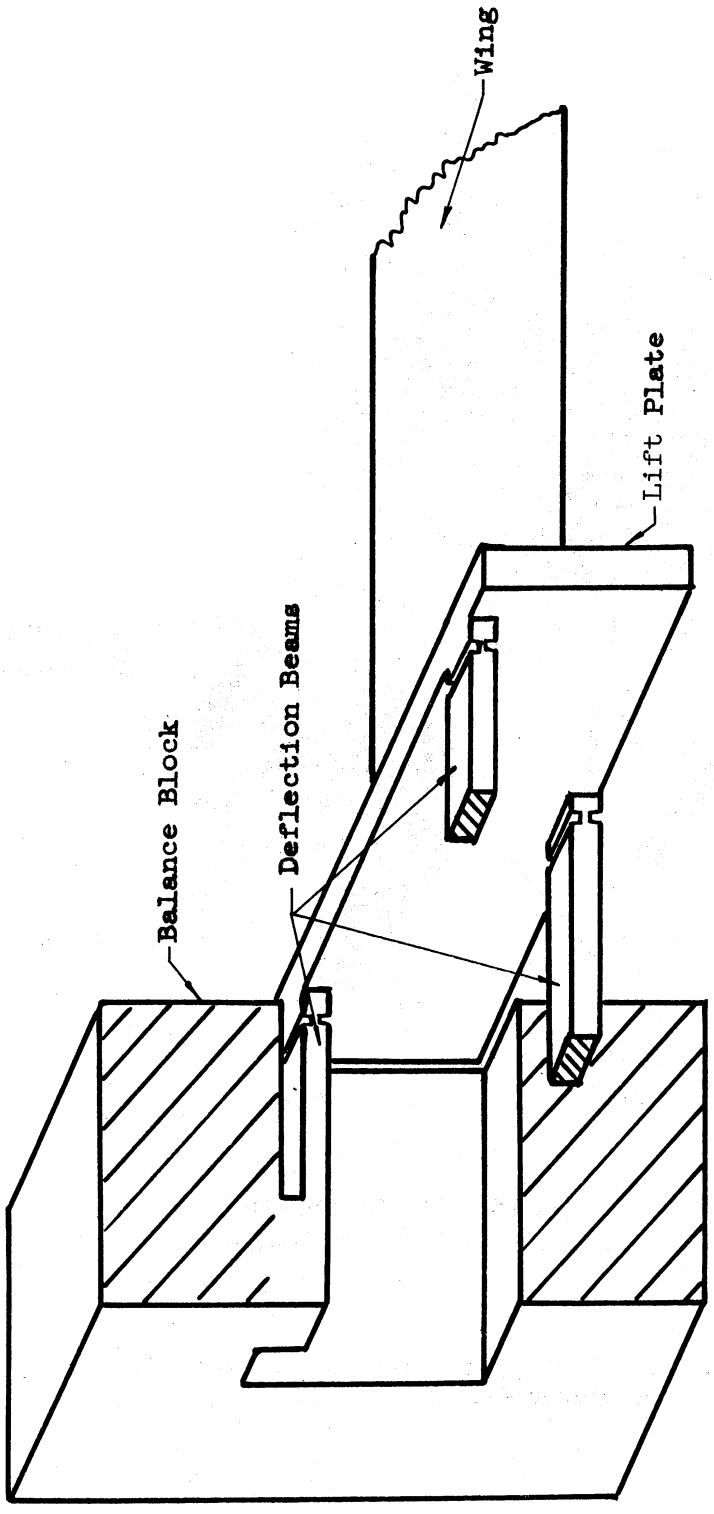

Figure 22-a. Cut-Away Sketch of Balance Block and Deflection Beams.

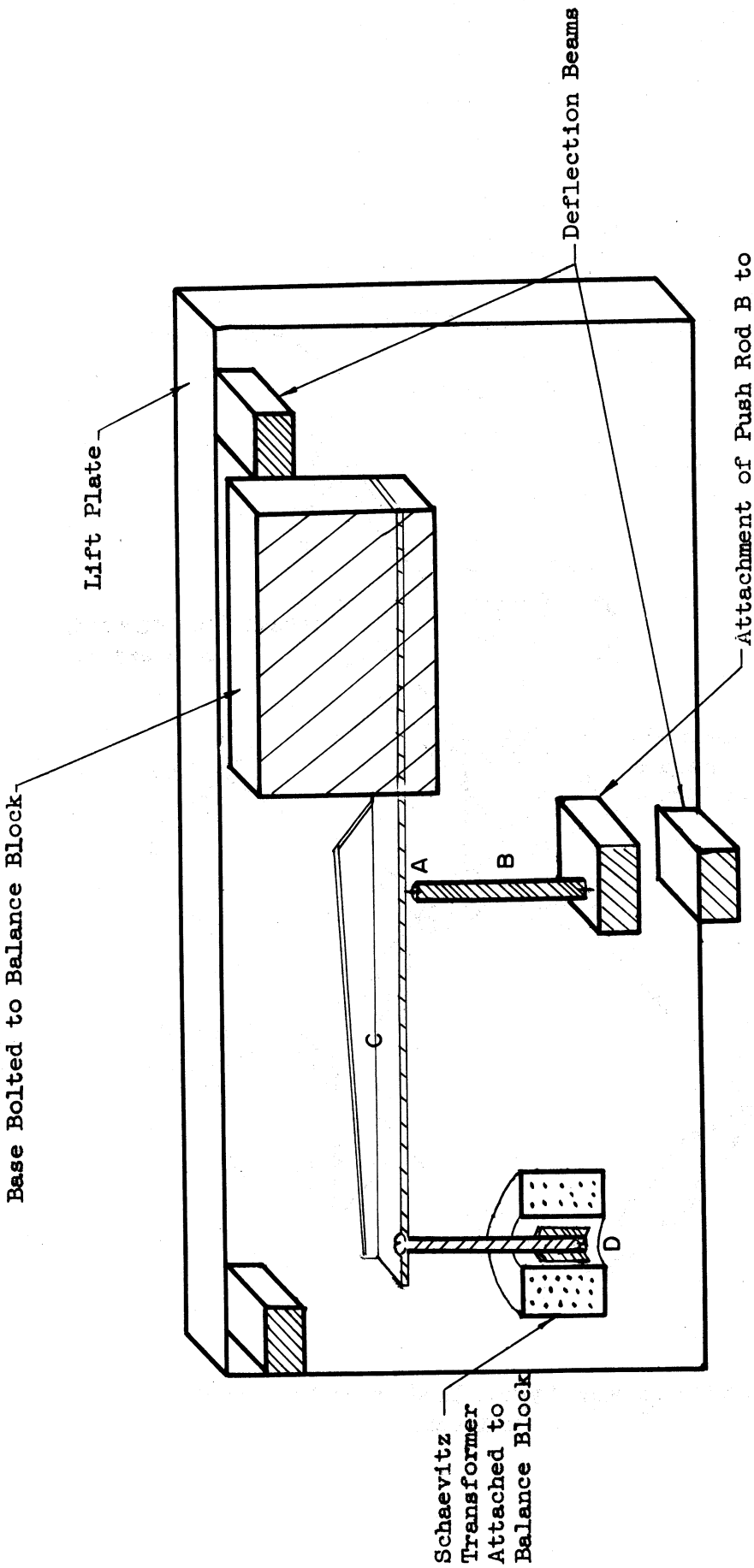

Figure 22-b. Cut-Away Showing Method of Measuring the Lift Displacement.

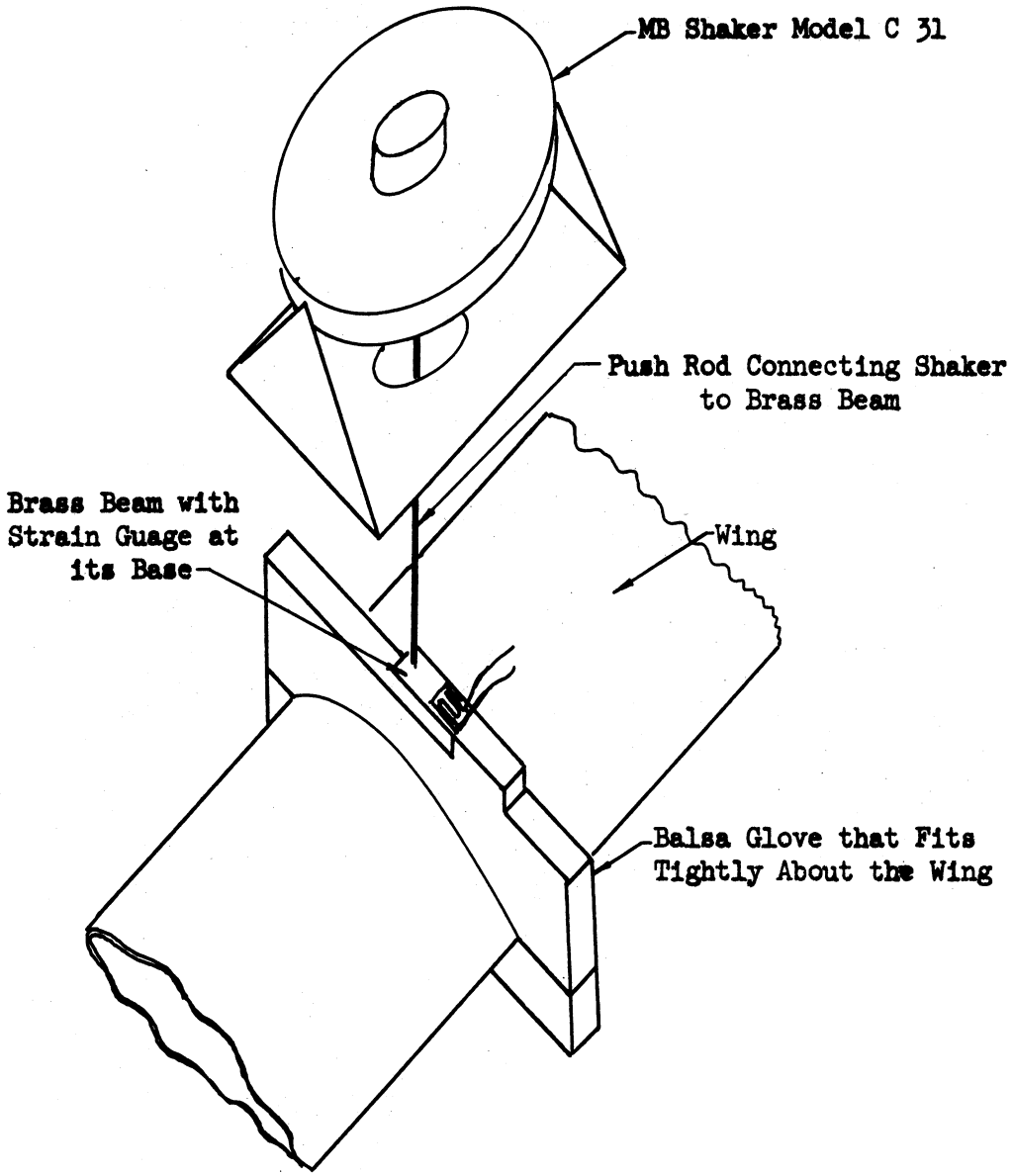

Figure 23. Sketch Showing System Used to Shake Wing for Dynamic Response Calibration Tests.

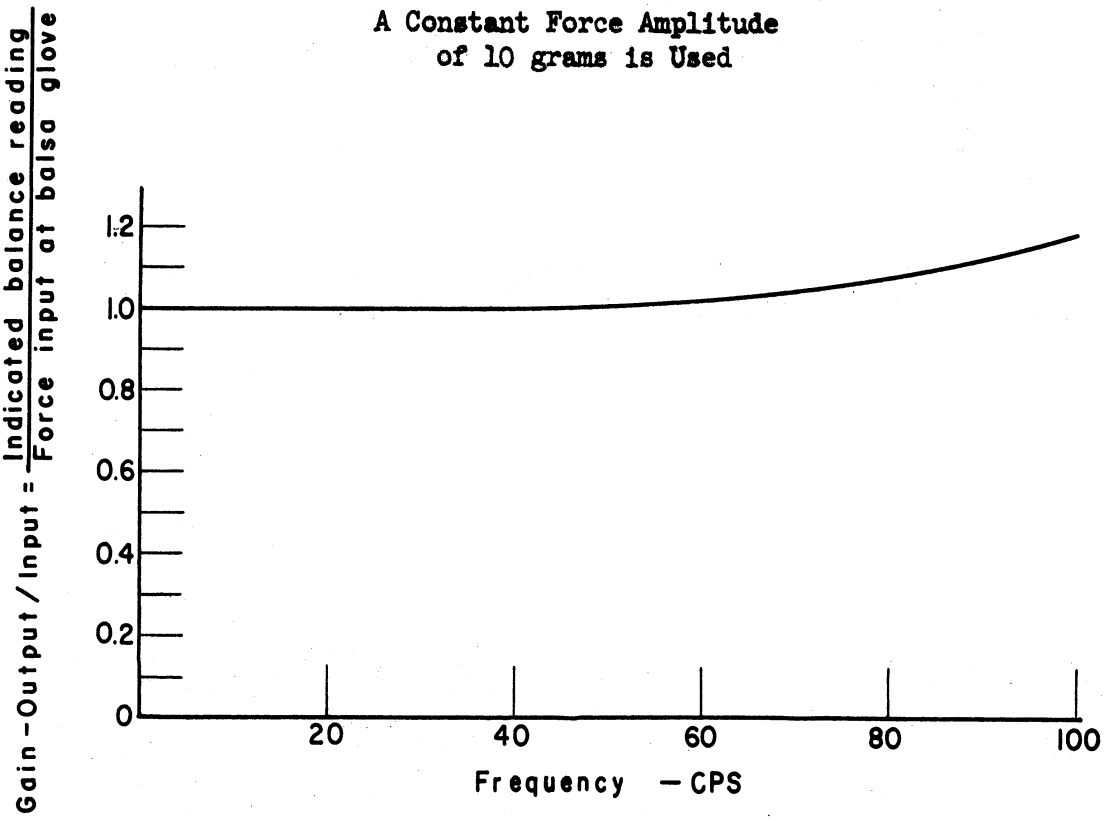

Figure 24. Frequency Response of Wing-Balance Combination. 21 x 29 Inch Model System.

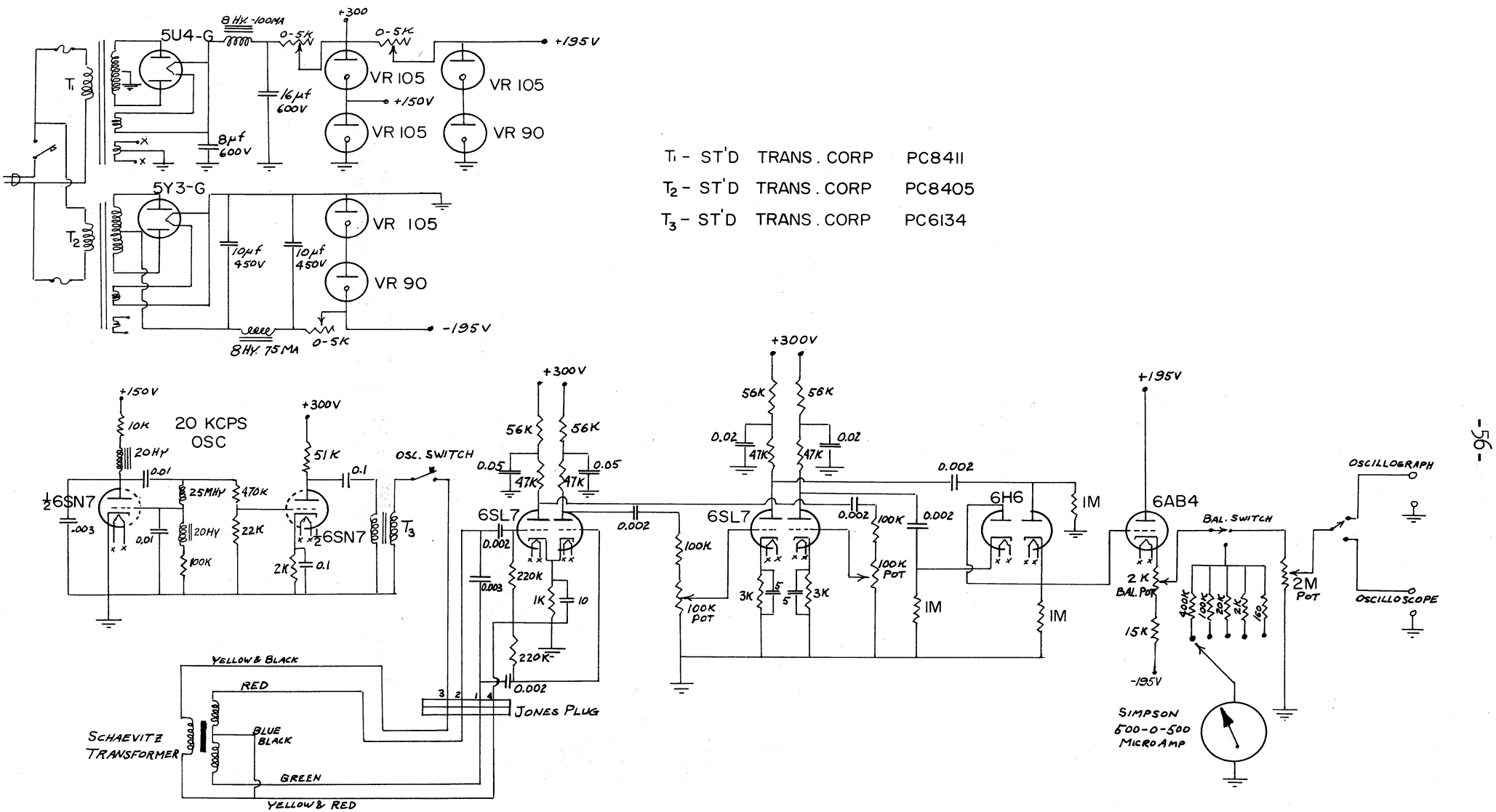

Figure 25 Electrical Circuit Used to Measure the Schaevitz Transformer Core Displacement

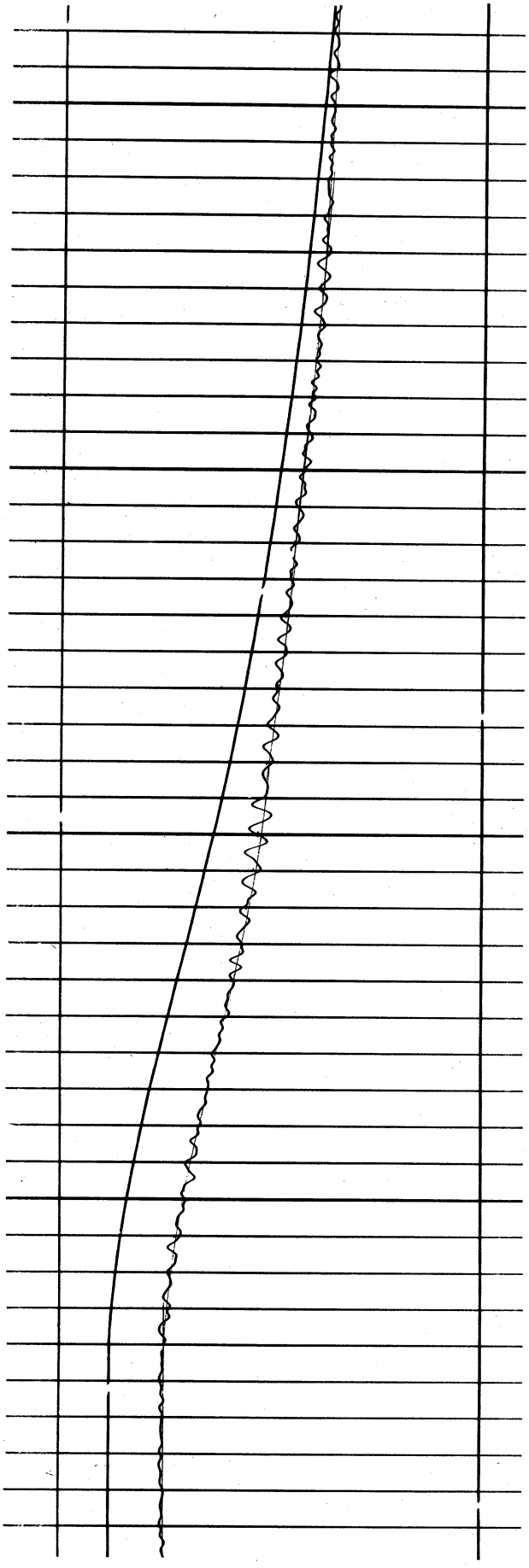

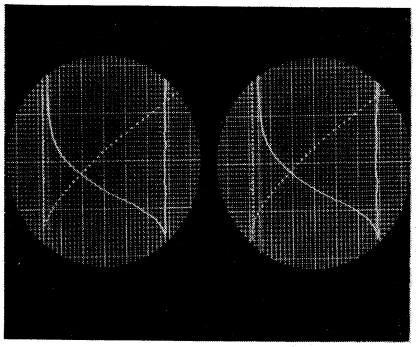

Figure 26. Typical Dynamic Test Traces